DOE/ER/03134--T1

DE82 005473

Lamont-Doherty Geological Observatory of Columbia University
Palisades, New York 10964

A COMPREHENSIVE STUDY OF THE SEISMOTECTONICS OF THE EASTERN ALEUTIAN ARC AND ASSOCIATED VOLCANIC SYSTEMS

Annual Progress Report

March 1, 1981 - Febuary 28, 1982

By

K.H. Jacob, E. Hauksson, L.R. Sykes, J. Davies, L. House, J. Mori, S. McNutt, D. Johnson, J. Peterson, J. Hauptman, M.A. Luckman, J. Beavan, and O. Perez

Prepared for the U.S. Department of Energy

Under Contract DE AS02-76ERO 3134

MGW

DISCLAIMER

TABLE OF CONTENTS

ABSTRACT

Assessment of the seismic potential for occurrence of great earthquakes in three seismic gaps (Shumagin Islands, Unalaska Island, and Yakataga-Kayak regions) has been completed. In the best-instrumented seismic gap in the Shumagin Islands region, the likelihood for a great earthquake within the next two decades is high. Analysis of earthquake data collected from a telemetered network operated in the Shumagin seismic gap shows near-quiescence in the shallow portion of the main thrust zone. The network data also indicate stress-patterns from composite focal mechanisms of events in the overriding plate, near the down-dip end of the thrust zone, and at subcrustal level within the descending Pacific lithosphere that are consistent with a presently locked state at the plate interface.

Stresses in the upper plane of the double-planed Benioff zone detected beneath the network indicate downdip tension; this stress inferred from composite focal mechanisms of network data is opposite to the downdip compression detected elsewhere in the eastern Aleutian arc in the upper plane of a weakly developed double Benioff zone as indicated by analysis of teleseismic data.

Installation of digital recording equipment at the central station of the Shumagin network, combined with interactive computer analysis at Lamont-Doherty of either digitally recorded or digitized analog seismic data has provided new research possibilities for studying seismic source properties, wave propagation in a laterally heterogeneous velocity structure of the subduction zone, and for seismically screening the root-zone and volcanic pile of Pavlof

volcano. High time-resolution data (0.01 sec), and wider frequency band-pass data (0.5-30 Hz) are now being collected. Seismic data for two eruptive sequences of Pavlof-volcano have been obtained. Interfacing of the Shumagin microseismic network with ten remote strong motion accelerographs for obtaining accurate strong motion trigger times has been completed.

2. INTRODUCTION

Lamont-Doherty Geological Observatory carries out a long-term comprehensive study of the seismotectonics of the eastern Aleutian arc, Alaska, and of its associated volcanic systems. This report describes completed research and related technical achievements during the first eight months, and outlines work in progress for the remaining four months of the contract period March 1, 1981 to February 28, 1982.

The remote region of the eastern Aleutian arc investigated in this study is tectonically characterized by the occurrence of very large infrequent thrust earthquakes along a subduction zone and associated volcanic arc. It is expected that within the next one or two decades a great thrust event will occur in the arc segment monitored by this study. The region studied requires attention from at least three points of view:

- research on the basic tectonic, seismic, and volcanic processes at a convergent plate margin;
- evaluation of the nature, origin, and accessability of energy resources in this tectonic environment which are potentially

present as (a) hydrocarbon resources in the shelf regions, (b) geothermal resources associated with the volcanic arc, and (c) dispersed coal deposites;

- evaluation of geologic hazards to the development of these energy resources and to energy-related installations (pipelines, storage tanks, etc.).

While this study focuses clearly on the first topic (basic seismologic and tectonic processes at a major segment of a convergent plate margin) the results described in this report directly affect both applied objectives (i.e., resources and hazards).

This comprehensive research project is aimed to provide both a broad overview of the seismicity and tectonics of a typical active subduction zone and associated volcanic arc as well as a detailed in-depth study of the microearthquake-activity and crustal deformation in this arc and of its associated volcanic systems. For the in-depth study we operate two regional telemetered networks of together 27 seismic stations covering a 600 km long arc segment; these networks include presently a 5-station network at and near Unalaska Island, a 14-station network in the Shumagin Islands seismic gap region to which attached is a subarray of 8 stations densely spaced on and around Pavlof Volcano on the western portion of the Alaska Peninsula. This Pavlof Volcano array monitors the seismicity associated with the magmatic processes in and beneath the most active volcano of the Aleutian arc, and of all of the U.S. The Pavlof study is aimed towards basic volcanic research which will, as a byproduct, contribute to assess the geothermal potential of Aleutian volcanoes, and of those in subduction zone tectonic environments in general.

The cost for operating the combined eastern Aleutian seismic networks is presently shared between this DOE-supported research program and a closely coordinated study under the Alaska Outer Continental Shelf Environmental Assessment Program (OCSEAP) administered by NOAA. OCSEAP urgently needed seismic hazards information for development of hydrocarbon resources on the vast Alaska shelf regions. The difficult logistic and climatic conditions and the vast expanse even of this small segment of the Aleutian arc (600 km long) require a level of effort both in manpower, logistic, and financial support which would by far exceed the fiscal limitations set for either of the two complimentary programs. It is therefore fortunate that both projects rely on the same seismological data base and hence have until now shared the high cost for network maintenance and technical realization. The NOAA/OCSEAP program is expected to terminate in September 1982. We expect a severe reduction in our network effort at this time which will have restrictive consequences for the research possibilities of also this project.

3. HIGHLIGHTS OF RESEARCH AND TECHNICAL ACHIEVEMENTS

- Completion of assessing the seismic potentials in the Shumagin, Unalaska and Yakataga seismic gaps and publication of results in a sequence of five papers.

- Near-completion of seismotectonic studies of the eastern Aleutians and of the central Gulf of Alaska by obtaining more than 40 new focal mechanism solutions using teleseismic data.

- Completion of study of the fine seismic structure and stress orientations in the double-planed dipping seismic zone beneath the Shumagin seismic array.

- A study into the importance of thermal stresses for the formation of double-planed seismic zones in subducting slabs of lithosphere.

- Installation of digital event-recording equipment for 32 channels of the Shumagin seismic network and Pavlov Volcano subarray.

- Switch-over to interactive digital network data analysis.

- Improved research possibilities due to higher time resolution, wider frequency bound and wider dynamic range of digital network data for the Pavlot volcano study and for determining lateral velocity structure beneath the Shumagin array.

- Recording of seismic activity associated with two eruptive sequences of Pavlof volcano.

This comprehensive study contains two distinct elements of reserach: a broad overview and detailed in-depth studies of special subjects. During this research period the effort towards providing a broad overview of the seismic and tectonic regime of the eastern Aleutian arc has probably peaked in its research output. The extensive analysis of the history of large earthquakes in the Aleutian

arc (Sykes et al., 1980; Sykes et al., 1981) of the tectonic setting and seismic potential for great earthquakes in the near future for the Shumagin seismic gap (Davies et al., 1981), for the Yakataga seismic gap (McCann et al., 1980; Perez and Jacob, 1980) and for the possible Unalaska seismic gap (House et al., 1981) are the prime examples of research results contributing to this broad overview. Work in progres by House and Jacob (1982) using teleseismic data and focal mechanism solutions to elucidate the shallow and intermediate depth subduction process in the eastern Aleutian arc, a similar attempt by Jacob and Perez (1982) for the central Gulf of Alaska, and by House and Jacob (1981) for the role of thermal stresses for the formation of double-planed dipping seismic zones also evolved from the past emphasis on broad seismic and tectonic aspects of this project.

As we have been striding throughout the recent years to consistently improve the technical equipment of the seismic network and the technical quality of collected data, we finally have reached the point where a new era in this project is about to start. While we can expect gradually diminishing research return from the remaining historic and teleseismic data, we now embark on the usage of a new generation of digital network data with high time resolution, wider dynamic range, and wider frequency bandpass than ever before available.

Clearly, this new generation of seismic network data permits more than simple locating of earthquake hypocenters or of first-motion focal mechanism studies. We are now able to extract quantitative information from wave-form analysis on the seismic sources, elastic and non-elastic properties of the structures and media in the

subduction zone, and can extend arrival time analysis to those of converted phases and other indicators of laterally varying velocity structures. The technical development for improving the quality of network is not yet completed. Future developments will incorporate an increased number of sites with 3-component sensors, digital rather than analog data transmission from remote to central recording site, and long-term (2 to 3 year) power supply for remote sites to reduce servicing frequency of the remote stations.

For the Pavlof Volcano study the new direct digital or digitized analog recordings permit for the first time extraction of quantitative frequency information from volcano-seismic signals. Until recently most of our volcano research was restricted to inferences and conclusions from simple counts of volcano-seismic events and their distribution in time. This is the first research period in which digital data have become available. We are still only learning how to extract pertinent information from these new data. Clearly it will take some time to fully master the use of the new data sources. Therefore those results that are based on the new data are still few for the present report. But we clearly recognize the change in emphasis within this project from less quantitative, broad studies to more quantitative detailed tectonic, seismic and volcanic studies.

The subsequent paragraphs describe in some greater detail the research accomplishments and technical achievements of this last research period.

4. RESEARCH RESULTS AND PROGRESS

4.1 Pn-Velocity Studies (E. Hauksson)

The purpose of the Pn-velocity studies is to determine the apparent Pn-velocity of the upper mantle below the Shumagin network. An accurate determination of the Pn-velocity at the base of the arc and fore-arc crust above the shallow portion of the descending slab and the aseismic wedge, is needed, for example, to obtain better locations of earthquakes that occur within the lower part of the slab. In addition, the velocity data will hopefully permit us to test for velocity contrast between the aseismic wedge and the subducted slab at depths between 35 and 100 km and will provide constraints on the initial velocity structure that is needed in the future for three-dimensional velocity inversions. Currently this work is in progress and below we describe the method of data analysis and some preliminary results.

Method of data analysis. The data set that we are utilizing for the Pn velocity study consist of approximately 30 earthquakes ($4.0 < M \leq 5.5$) that have occurred outside of the Shumagin network at distances from 200 km to 1200 km. These events are located along the Aleutian arc and were all recorded by most stations in the network in 1980 and 1981. The time-term method will be used to determine relative station residuals and the Pn-velocity. The locations of the events can be taken from the PDE bulletins since possible sources of error, as for example, origin time, epicenter or depth do not enter into the determination of Pn-velocity when the time-term method is used (McCollon and Crosson, 1975).

The time-term method has been applied in somewhat different ways by numerous investigators to determine Pn velocity. As an initial approach we have chosen to apply the technique of McCollon and Crosson (1975), since the geometry of both cases appears to be similar. First the apparent velocity is determined for each event from the equation,

$$t_i - d_i = d + \frac{\Delta_i}{v} \qquad (1)$$

where t_i is the travel time to the i-th station, d_i is a station delay at the i-th station and Δ_i is the epicentral distance. The equation (1) is solved by weighted least squares with respect to d, a constant delay and v, the apparent velocity to estimate if the set of observations is within the Pn-velocity range. Events with large errors can thus be corrected or eliminated from the data set.

Second, the time-term method is applied to calculate the refractor velocity and relative station delays from,

$$t_{ij} = d_i + d_j + \frac{\Delta_{ij}}{v} \qquad (2)$$

The above equation is also solved by weighted least squares for the unknowns d_i, d_j and v, where i = 1, 2,...k and k is the number of stations. The station and event delays are d_i and d_j, respectively, and j = 1, 2,...l where l is the number of events.

Third, the relative station delays from equation (2) are used to solve equation (1) again and obtain more accurate values for the apparent Pn-velocity. This iteration is repeated until an accurate estimate of the Pn-velocity has been determined.

Our results will probably be complicated by 1) lateral variations, 2) anisotropy, and 3) anomalous station delays. Lateral variations can either be caused by a dipping moho or a curved moho or possibly by an inhomogeneous upper mantle. If the data are extensive enough some of these different possibilities can be resolved and estimated in a quantitative way (see, for example, Vetter and Minster, 1981). A possible anisotropy would be related to the properties of the upper mantle material and could be estimated using a variety of different techniques. We expect to find anomalous station delays close to Pavlof volcano because of the possible existence of a magma reservoir. Such stations can be removed from the main data set while we unravel the general Pn-velocity structure of the region.

Preliminary results. Approximately 20 events have been digitized from the analog Teac tapes onto computer compatible tapes. The P=arrivals have been picked interactively with an acuracy better than 1/20 of a second. The next step will consist of writing and implementing the computer programs that are needed for analyzing the data as described previously. In Figure 1 we show data from two different events. We used the hypocenter location program, HYPOINVERSE to calculate the travel time from the known PDE hypocenter and origin time to the respective seismic station. The calculated and observed travel-time delays were reduced by a factor of $\Delta/7.9$ (sec) to facilitate plotting of the data. Data from both events indicate that

stations (such as BKJ, CNB, and SNK) located close to the trench are associated with small station delays (<0.3 sec) and stations located far away from the trench axis (such as FSP, BAL, and PN4) are associated with large (>1 sec) station delays. This preliminary list of the data thus indicates that the data can resolve relative station delays, Pn-velocity and possible lateral variations in the shape of the moho.

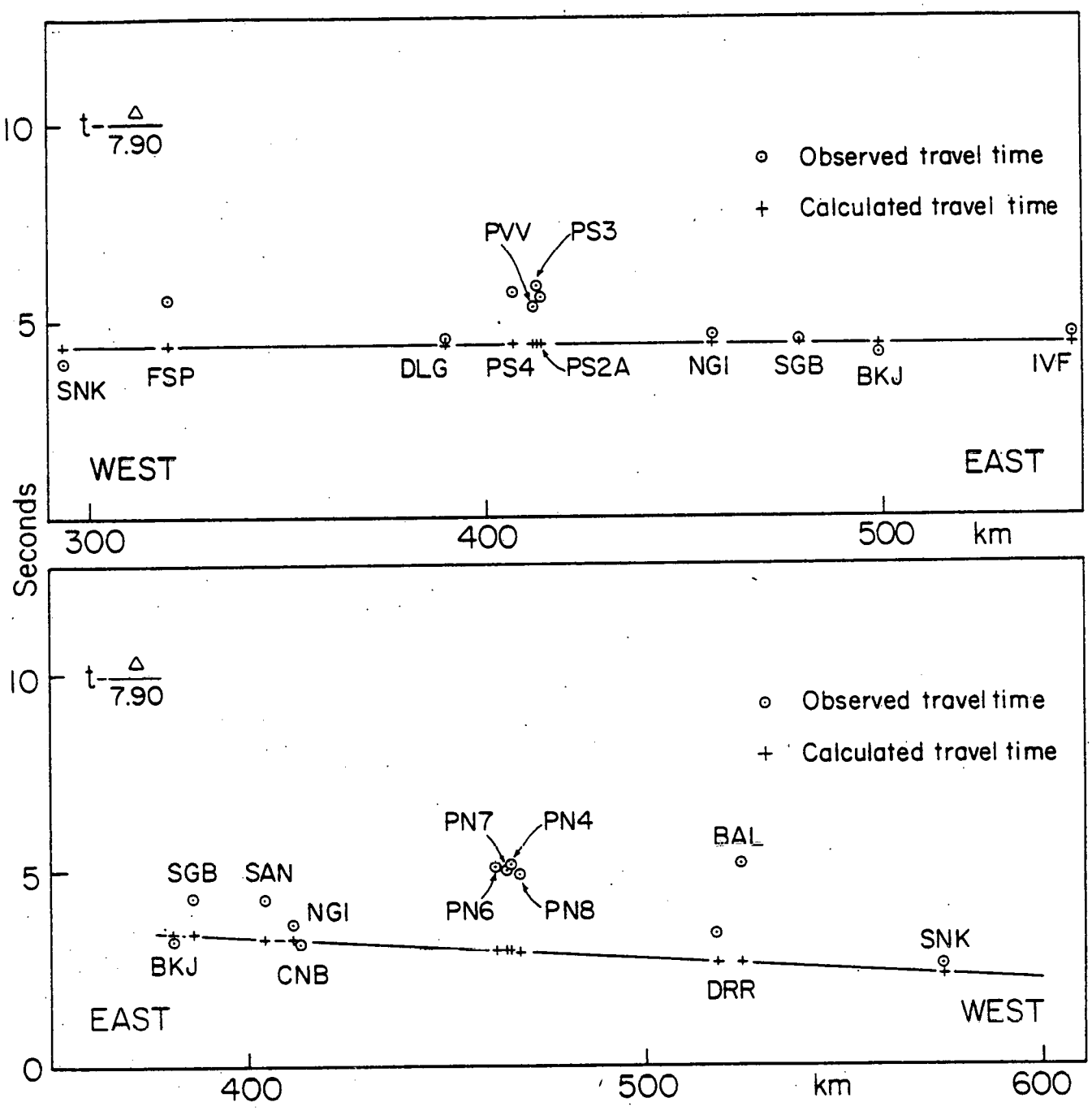

Figure 1. Reduced travel time curves for (a) an event with origin date and epicenters 81/01/20, 55n51.00 and 155w 44.00 and (b) an event from 81/06/05, 52n15.50 and 165w11.20. The stations shown constitute the Shumagin network and the Pavlof array.

4.2 Tests on Velocity Models and Lateral Heterogeneities (K. Jacob and J. Peterson)

Presently we use a flat-layered earth model $V_{po}(h)$ (Table 1) for P-velocities and a constant Poisson ratio (implying a constant V_p/V_s ratio of 1.73) to locate earthquakes beneath the Shumagin Islands network. The inferred thermal and tectonic structures of subduction zones suggest that instead a two- or three-dimensional velocity structure is required to obtain unbiased earthquake locations and to describe correctly geometrical wave propagation through the structures.

Rather than immediately solving for a 3-D velocity structure simultaneously during the locating procedure for large numbers of earthquakes, we carried out a simple test to see whether or not the travel time data collected by the Shumagin network in fact contain clearly discernable information on the three-dimensionality of the velocity structure. This simple test is described below and its result indicates that the Shumagin seismic data indeed contain sufficient information to warrant a rigorous inversion for lateral velocity heterogeneities.

The data base for this test consists of the carefully screened and selected hypocenters shown in Figure 2 (Reyners and Coles, 1981) that have good depth control and obey several other constraints. They were located using the flat layered earth model (Table 1) and routine locating programs (HYPOINVERSE (Klein, 1978), and HYPOELLIPSE (Lahr, 1980)).

Despite their likely bias in location due to ignoring lateral velocity perturbations in the subductio zone, we assume for this test that the origin parameters truthfully describe these sources in time and space. We then define an average velocity $v(h) = t_p/s$ for each event-station pair whereby t_p is the P-travel time and s the straight-line distance $s = (h^2+d^2)^{1/2}$ between event at depth h and station at epicenter distance d, thus assuming (ignoring reality) a homogeneous half-space velocity between surface and depth h for each event. These assumed velocities are calculated in two different ways: (a) using origin times from hypocenter locating procedures and (b) using origin times from Wadati diagrams using a method and program developed by Nicholson and Simpson (1981). Both average velocities are displayed for each event (solid dots and crosses, respectively) as a function of hypocenter depth, h, for four stations (Figure 3a). We then obtain smoothed average velocities using a Δh=5 km moving window. These smoothed average velocities V_{pa} are shown by the solid linesin Figure 3a. From the smoothed average velocities we can derive interval velocities by a backstripping procedure, starting at depth h=0 and working to depth h = 120 km in intervals of Δh = 5 km:

$$V_p[(h,\ h+\Delta h) = \Delta h\ [(h+\Delta h)/V_{pa}(h+\Delta h) - h/V_{pa}(h)]^{-1}$$

These backstripped interval velocities are plotted as a function of depth h (Figure 3b) for the same four stations.

Note that this interval velocity, V_p, although treated as if only a function of depth, reflects in fact lateral heterogeneities that are sampled between events at depth h and $h+\Delta h$ and the respective

observing station at the surface h=0. Hence, this variable V_p is only apparently and not truly an interval velocity. This effect is clearly discernable from the apparent lowering of interval velocity V_p at depths deeper than h=40 km for station NGI (Figure 3b). For these depths, ray paths from events to NGI suddenly penetrate through the aseismic wedge that lies above the dipping seismic (Benioff) zone and below the seemingly active shallow crust of the arc and forearc, arcward of the aseismic front. This aseismic wedge apparently contains material with velocities lower than the material at the same depth but associated with the cold descending Pacific plate, seaward or trenchward of the aseismic front.

Hence, while this test does not correctly attribute interval velocities to their associated depth-range and structural features, it clearly shows a strong variability of V_p as a function of depth, that also varies from station to station. For comparison to the derived interval velocities we also show (Figure 3b) the flat-layered earth-model $V_{po}(h)$ presently used for locating events. It is apparent from this comparison that in an average sense the layered model adequately describes the crustal and upper mantle velocity surprisingly well. Nevertheless, lateral variations of V_p velocities beneath the Shumagin array are substantial, and they must be accounted for if absolute hypocenter locations are going to be freed from systematic biases.

In conclusion, this simple test provides evidence that the travel time data from events beneath the Shumagin seismic network contain strong evidence for lateral velocity heterogeneities. It appears that a rigorous velocity inversion procedure including use of a

THIS PAGE

WAS INTENTIONALLY

LEFT BLANK

3-d-ray tracing program for forward calculations, incorporating lateral perturbations, is warranted. The presently available data set may be sufficient for constraining only a two-dimensional velocity model using, however, three-dimensional ray paths. If a truly three dimensional velocity model is required to describe the travel time observations, a much greater data set will be required. The presently digitally recorded travel time data from recent events provide such information and are of the sufficient high quality.

TABLE 1

Flat-Layered P-Velocity Model for the Shumagin Islands Array Region

P-Wave Velocity of Layer (km s^{-1})	Depth to Top of Layer (km)
3.44	0.00
5.56	1.79
6.06	3.65
6.72	10.18
7.61	22.63
7.90	38.51
8.26	90.19

A ratio of P-wave velocity to S-wave velocity of 1.73 was adopted for all layers.

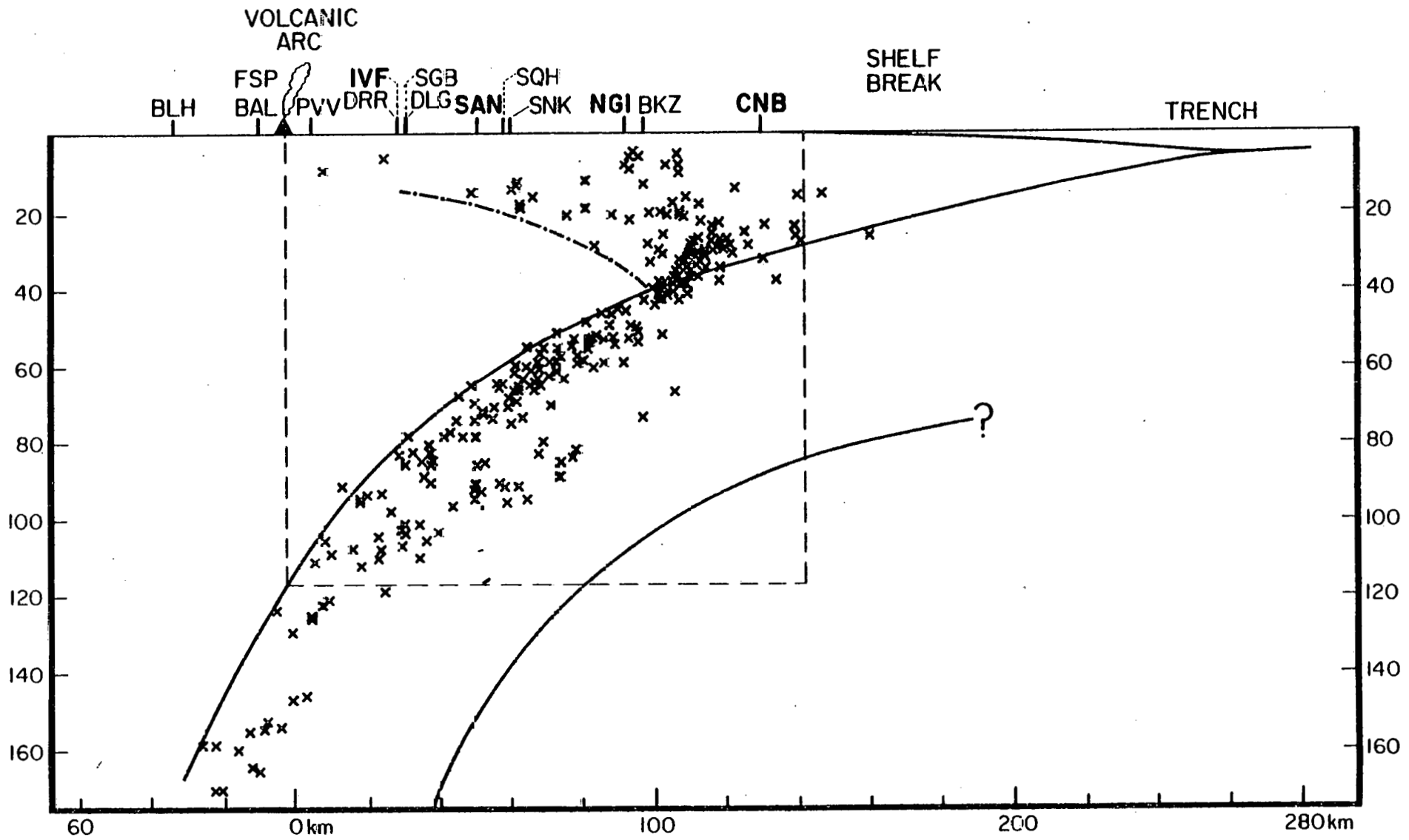

Figure 2. Cross sectional view of a set of well-located earthquakes (Reyners and Coles, 1981) that was used to test velocity models for significant lateral variations. Only those events (crosses) within the box outlined by the broken line are used. The four stations (IVF, SAN, NGI, and CNB) for which velocity functions are displayed in Figure 3 are marked in heavy lettering. The top of the inferred aseismic wedge is indicated by a dashed-dotted line. Where it connects to the inferred upper surface of the descending Pacific plate, 40 km beneath station NGI, the 'aseismic front' is located. (No vertical exaggeration).

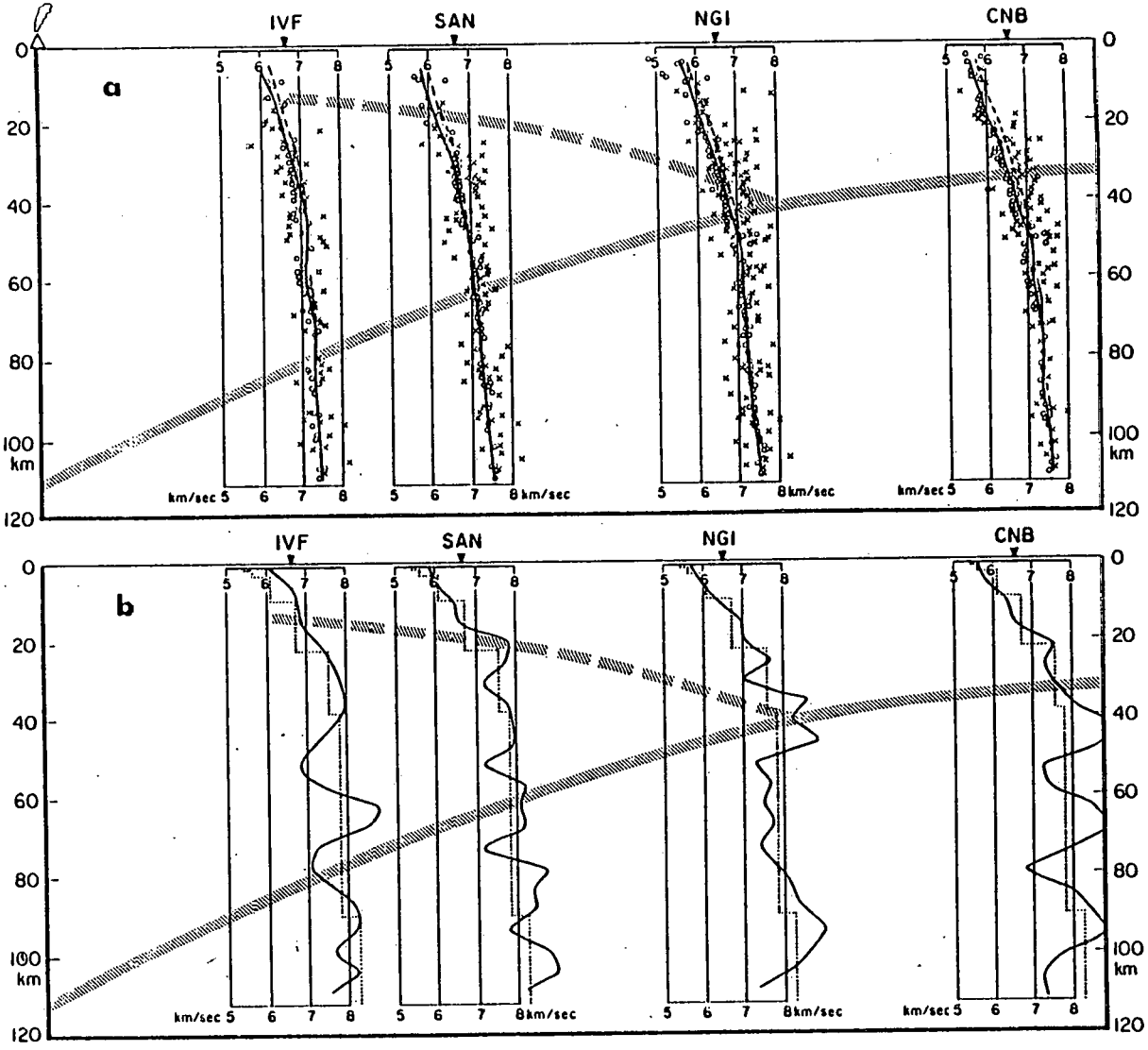

Figure 3. (a) Half-space P velocities inferred from hypo-locations (circles) and Wadati-diagrams (crosses) beneath four stations and from some 200 earthquakes. Solid line is smoothed (5 km-window in depth) half-space velocity for hypo-derived velocities. Broken-line is half-space velocity derived from interval velocity shown in Figure 3b. Shaded signatures indicate inferred upper slab surface and roof of the aseismic wedge, respectively. Horizontal spread is about 140 km (i.e., horizontal exaggeration is about 2 to 1). (b) Interval P-velocities derived beneath four stations from hypo-half-space velocities (solid lines) and those used presently to locate earthquakes using a flat-layered model (dotted curves) of Table 1.

4.3 Fine Structure of the Dipping Seismic Zone in the Shumagin Islands (M. Reyners and K. Coles)

This study, using a highly restrictive set of well located earthquakes beneath the Shumagin Islands seismic network, has now been completed (Reyners and Coles, 1981). The new results, additional to those previously reported, concern sets of composite focal mechanisms from events at the plate interface, within the overriding plate, and in the downgoing plate in which a dipping double seismic zone has been identified.

Composite fault-plane solutions for subsets of the microearthquake activity which give consistent focal mechanisms are shown in Figure 4, together with a depth section showing the subsets themselves. Solution C in Figure 4 shows a down dip tension axis in the upper plane of the double seismic zone, rather than the down-dip compression that would be consistent with a simple unbending model (Engdahl and Scholz, 1977). Solutions D and E, from the lower plane of the double-planed dipping seismic zone, have no simple explanation in terms of down-dip stresses. It may be that, because the plate interface is currently locked at shallower depths, slab pull is overprinting unbending stresses; such an interpretation is consistent with the curretly high seismic potential inferred for the region (Davies et al., 1981).

The composite fault-plane solution for the concentrated activity shallower than 45 km (solution A in Figure 4) indicates thrust faulting. As can be seen in Figure 4A, the P axis of this composite fault-plane solution is near-horizontal, and its azimuth (330°) is

very similar to the azimuth of plate convergence predicted by the RM2 model of Minster and Jordan (1978) for the region of the Shumagin array (329°). In addition, one nodal plane of the solution is subparallel to the dipping zone defined by the 25-45 km deep activity. Landward of this activity, microearthquakes in the overlying North American plate show a strike-slip mechanism (see Figure 4B), with the P-axis again near-horizontal and oriented in the direction of plate convergence. This result is consistent with the interpretation that the plate interface in the region of the Shumagin Islands is currently locked, with stresses due to plate convergence being transmitted to the overlying plate.

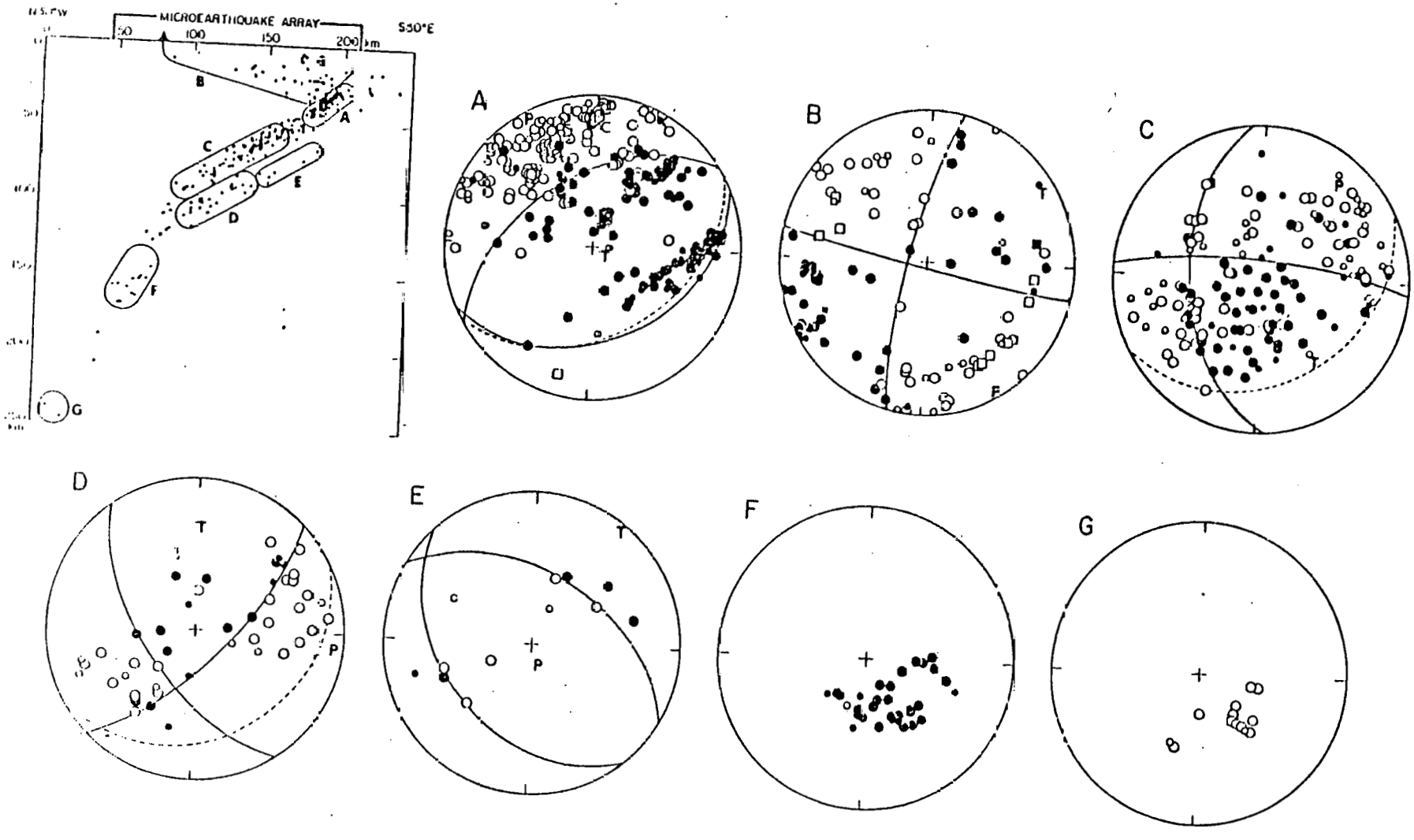

Figure 4. Subsets of microearthquakes for which composite fault-plane solutions have been determined (top left-hand diagram), together with the corresponding solutions. All stereograms are equal-area projections of the upper focal hemisphere. Open symbols represent dilatational, and solid symbols compressional P-wave first motions. Circles represent arrivals leaving the focus in an upward direction; squares are critically refracted arrivals projected from the lower hemisphere. Smaller symbols indicate less reliable readings,

4.4 Thermal Stresses in Subducting Lithosphere: Consequences for Double Seismic Zones (L. House and K. Jacob)

The discovery of double-planed zones of intermediate-depth seismicity associated with subducting oceanic lithosphere (Sykes, 1966; Veith, 1974, 1977; Isacks and Barazangi, 1977; Engdahl and Scholz, 1977; Hasegawa et al., 1979; Samowitz and Forsyth, 1981) has generated lively discussion about the origin and distribution of stresses in descending plates. So far, four mechanisms have been proposed to explain double seismic zones: a change of phase, from olivine to spinel, in the descending plate (Veith, 1974); unbending of the subduction plate (Isacks and Barazangi, 1977; Engdahl and Scholz, 1977); sagging of the subducting plate (Sleep, 1979); and thermal expansion as the descending plate is warmed by the surrounding mantle. Since double seismic zones have been identified beneath only a few island arcs, they do not appear to be a universal feature of downgoing slabs (Fujita and Kanamori, 1981). In addition, the best-documented double seismic zone occurs beneath northeastern Honshu within a portion of the downgoing plate that appears to be straight (see Figure 5). Our subsequent discussion and evaluation of possible mechanisms for producing double seismic zones will refer in particular to that beneath northeast Honshu.

The phase change hypothesis has difficulty accounting for the shallowest depth at which the double zone is observed (Fujita and Kanamori, 1981). Unbending of the plate, while able to account for the polarities of focal mechanisms and separation between the two zones, does not appear to be, by itself, able to account for the

length over which the double zone is observed, or for the observation of the double zone within the apparently straight descending plate. In addition, it is not clear why unbending of the plate should produce a well defined double zone of seismicity when the bending of the plate did not produce such a feature. A third hypothesis, sagging, also appeals to a mechanical process to produce the observed double zone of seismicity (Sleep, 1979). Unfortunately, sagging is a hypothesis that is untestable, since the present-day shape of the plate does not necessarily establish whether it is sagging or not.

Thermal stresses within the descending slab have been proposed as a mechanism for producing the polarities and separation of strsses inferred from double seismic zones (Yang et al., 1977; Hamaguchi et al., 1981). We seek to evaluate further the possible role of thermal stresses in producing double seismic zones.

We start from a simple model of temperatures in the downgoing plate as calculated by Toksöz et al. (1971) (see Figure 6). From this temperature distribution, we use a thin plate assumption (Timoshenko and Goodier, 1970) to obtain estimates of thermally induced stresses within the down-going plate. The results are encouraging; not only do the thermally induced stresses have the appropriate polarities, but they also appear to have about the same separation (≈30 km) as the two zones of seismicity at the shallow end (see Figures 6 and 7). There is also a suggestion of a merging of the zones of maximum tension and compression at greater depths.

The state of stress within descending slabs of lithosphere likely is a sum of many different contributions. Stresses derived from unbending and the negative buoyancy, among other sources, may, in

general, be much larger than the thermally-derived stresses computed here. Nevertheless, in some slabs, the sum of the stresses that result from the other effects may be small enough that thermoelastic stresses could significantly influence the state of stress within the slabs, and could produce two subparallel zones of seismicity. If thermoelastic stresses do play a large role in producing double-planed zones of seismicity within some downgoing slabs, then seismologic observations may help to constrain models of the temperature distributions within downgoing plates.

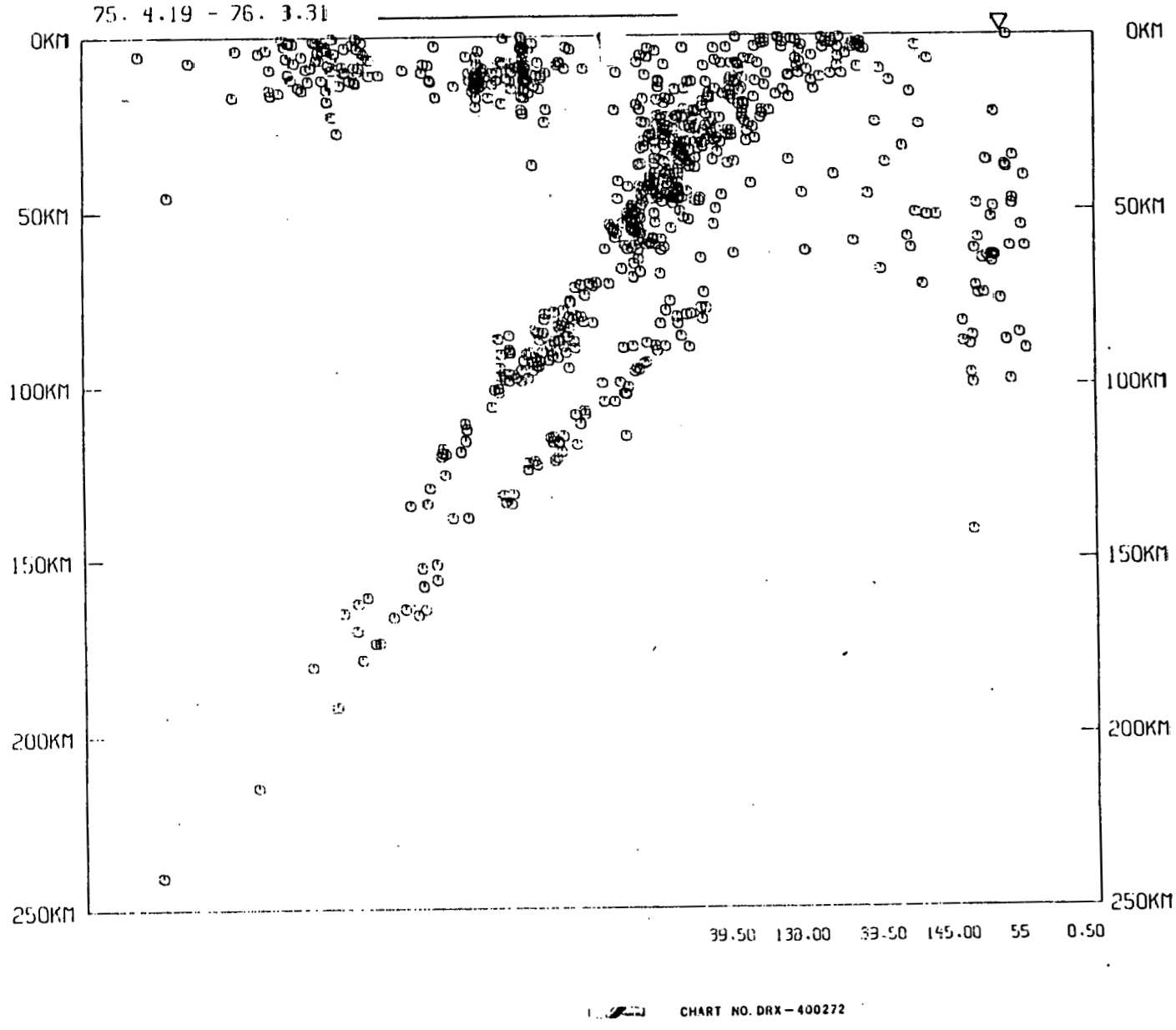

Figure 5. Double seismic zone beneath northeast Honshu, Japan. Figure shows microearthquakes located by a network operated by Tohoku University. The bar in the figure shows the projection of land areas of the island of Honshu, and the inverted triangle shows the location of the Japan Trench. Vertical exaggeration is 2:1. (From Hasegawa et al., 1978).

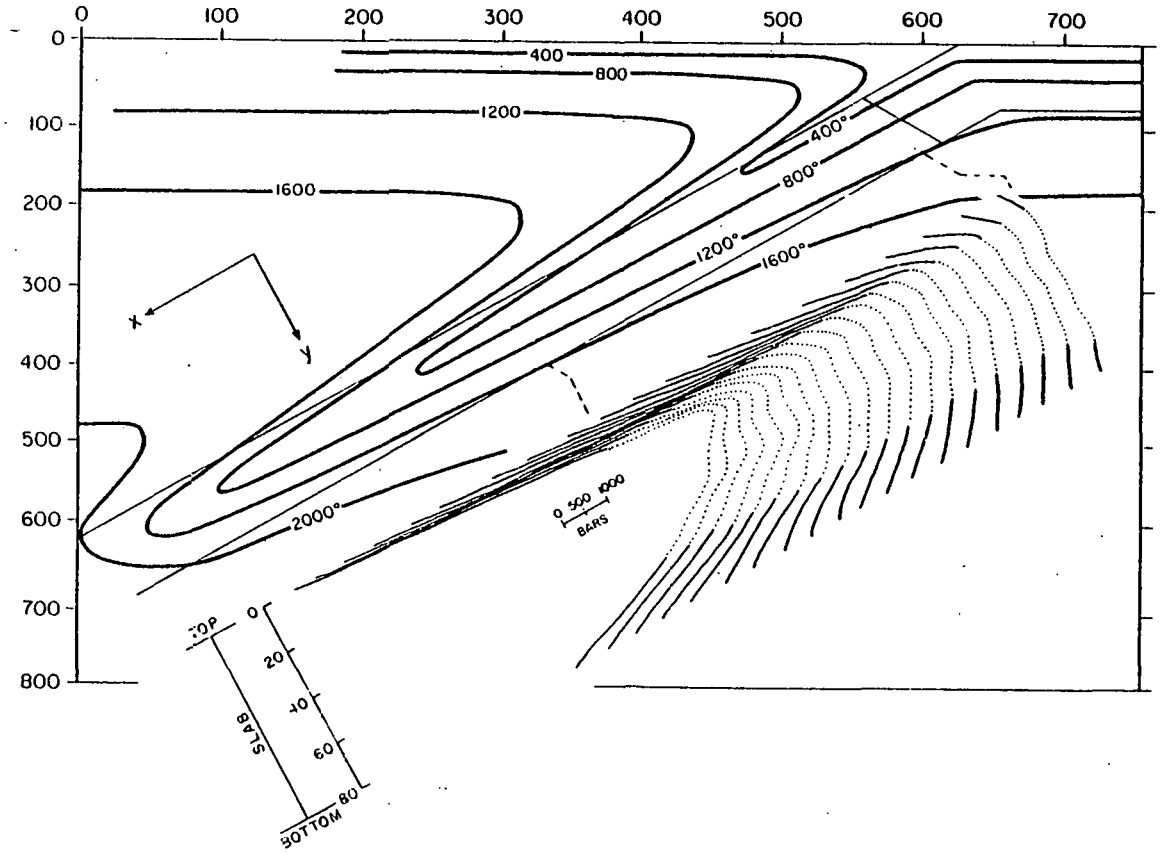

Figure 6. Thermal model of the descending lithospheric slab and cumulative thermoelastic stresses obtained from it. Isotherms (in °C) are derived from numerical modelling of an 80 km thick slab that dips at 45° and subducts at a rate of 8 cm/yr (after Toksöz et al.). The coordinate system used is noted in the inset, upper left; y=0 at the center of the slab; the z axis points out of the page (along the strike of the slab). Cumulative thermoelastic stresses calculated for the 80 km thick slab model (no relaxation) are inset in the lower right. Each successively deeper profile is the sum of the stresses from the previous profile, plus the increment of stresses developed between the profiles. Note the difference in the y scale from the main figure. Tensional stresses are indicated by the dotted portions; compressional by the solid lines. Note that cumulative tensional stresses of more than 2 kbar are reached only about 20 km interior to the slab from where cumulative compressional stresses of 6 kbar are developed. A grid spacing of 10 km in the y direction was used in the computations; details with a comparable wavelength are unreliable. Note the horizontal exaggeration of about 1.7 in the main figure. Temperature profiles were taken in a direction normal to the surface of the downgoing plate, but, because of the horizontal exaggeration of the main figure, the lines of the profiles appears skewed. The y axis is directed normal to the plate.

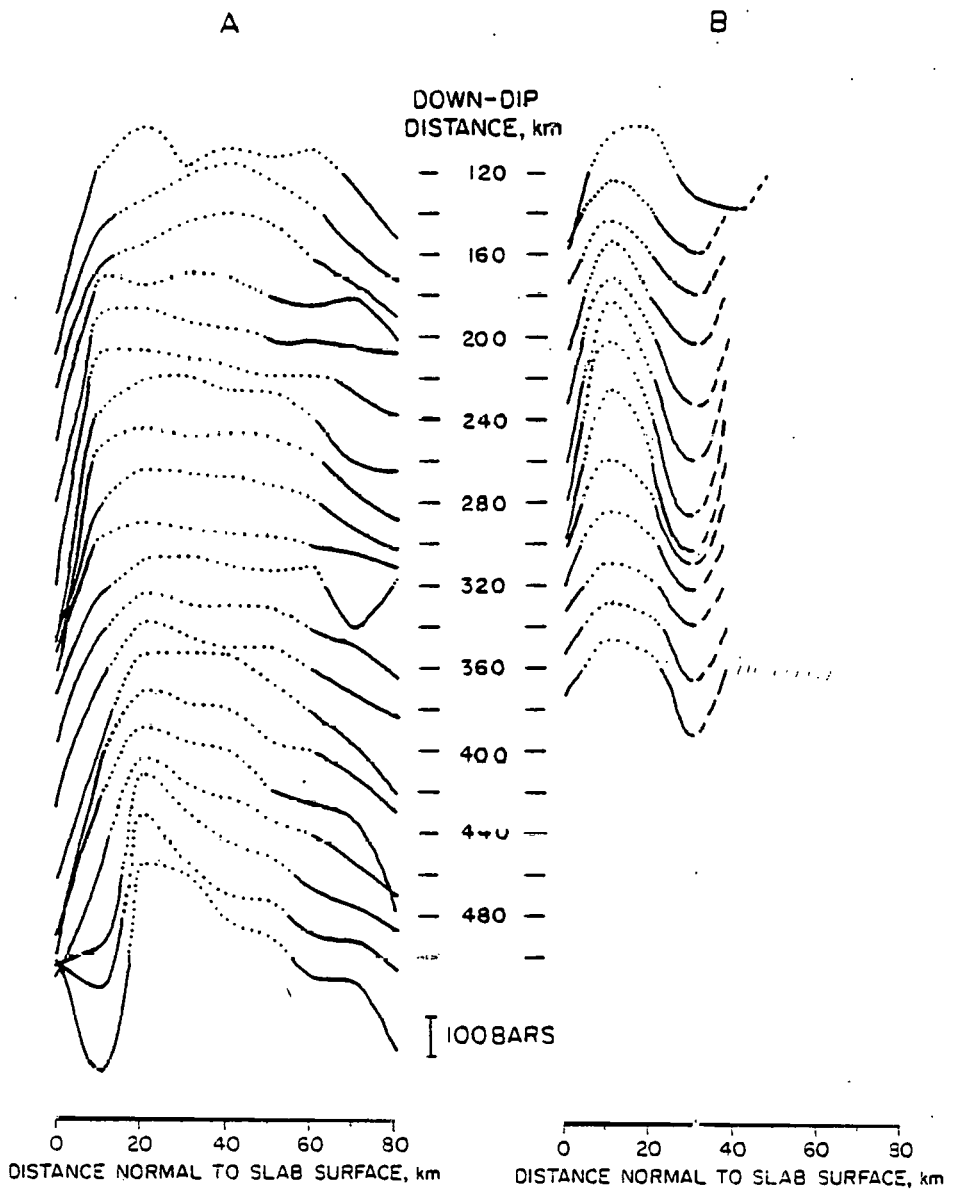

Figure 7. (a) Incremental thermoelastic stress profiles calculated with an 80 km thick elastic slab. As in Figure 6, the dotted portions of each profile are tensional, the solid portions compressional. Features with a wavelength comparable to or smaller than the grid spacing (10 km) are unreliably determined. Note the narrowing of the separation between the maximum tension and compression toward the lower profiles. (b) As 7a except that relaxation by high temperature creep (see text) is allowed to reduce the effective elastic thickness of the slab, when relaxation approximately equals or exceeds the thermal strain rates ($\sim 10^{-18} s^{-1}$). Portions of the slab where relaxation has occurred are shaded. Dashed portions of the stress profiles indicate regions of transition between elastic and relaxed portions of the slab. Stress profiles are omitted below a down-dip length of 360 km; only a 20 km thickness of the lithosphere remains elastic and since temperatures are sampled at 10 km intervals, computed stresses would be unreliable.

4.5 Focal Mechanism Study in Central Gulf of Alaska and Interior Alaska (K. Jacob and O. Perez)

This study, still in progress, attempts to address the problem of stress transmission from the very wide, shallowly dipping plate boundary in the central Gulf of Alaska into the interior of the overriding plate in continental central Alaska. A total of 18 new and re-determined focal mechanisms have been completed (#1 to 18) and are plotted in Figure 8, together with several published ones (#19 to 23) for SE Alaska (Perez and Jacob, 1980). This summary figure indicates normal faulting near the trench, a surprising coexistence of normal and thrust faults in the vicinity of the main thrust zone beneath the Kodiak-Kenai shelf region, and down-dip tensional intermediate-depth events in the descending slab beneath the volcanic arc. Events in the overriding continental plate range from thrusting near Mt. McKinley, strike-slip in central Alaska to normal faulting near the Norton Bay-Seward Peninsula region.

Interpretation of these data is still incomplete as refinement of hypocentral depth is underway. Accurate depth may play an important role in correctly interpreting the tectonic role of these events as stress or strain indicators.

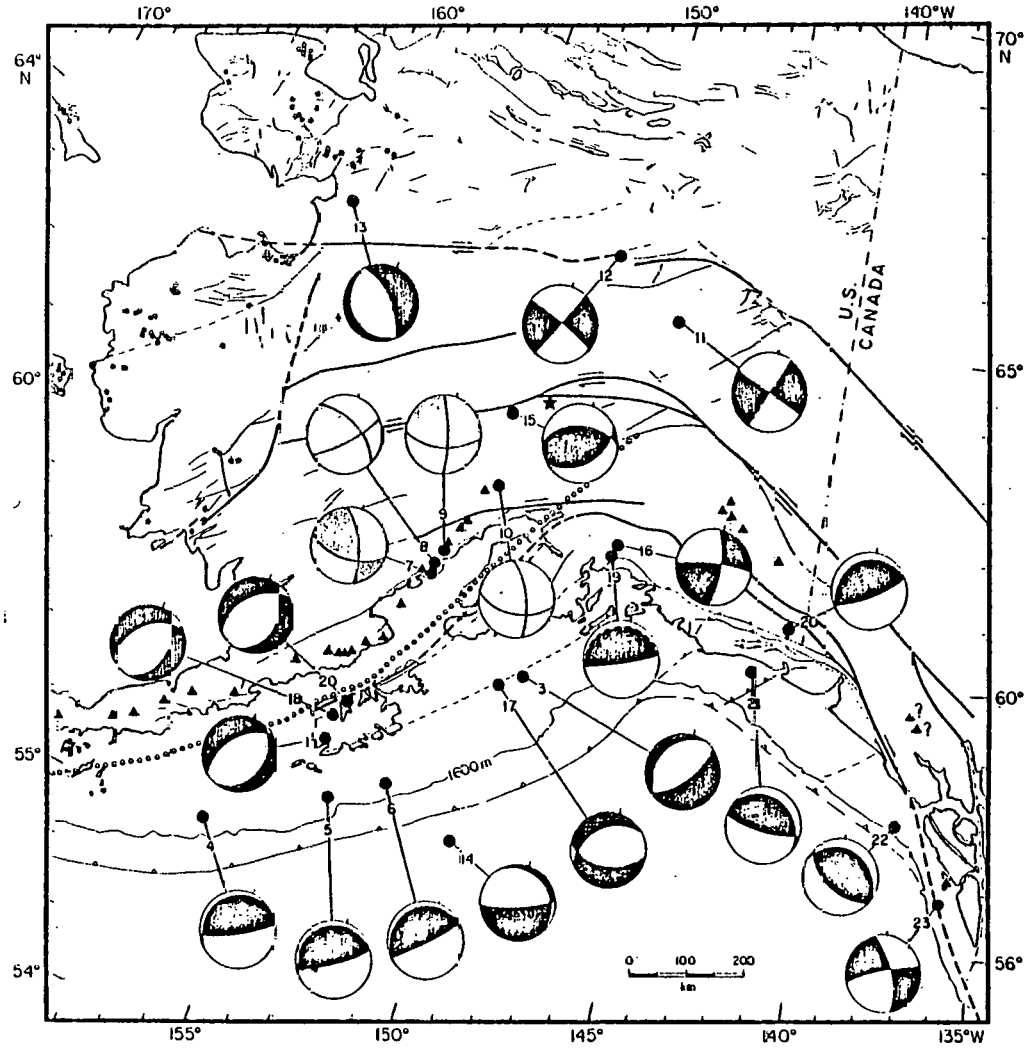

Figure 8. Focal mechanisms of 18 newly determined and 7 previously published (Perez and Jacob, 1980) solutions for the Gulf of Alaska and portions of interior Alaska. Thrust solutions (#4, 5, 6, 19, 20, 21, 22) dominate on the main plate-interface, but between them are dispersed a few normal faulting solutions (#1, 3, 17, 18, 20) which are spatially and tectonically distinct from normal faulting in the trench region of the descending plate (#14). Deformation in the overriding plate ranges from thrusting (#15) to strike-slip (#11, 12) to normal faulting (#13) progressing in this sequence away from the primary plate boundary. At intermediate depths down-dip tension appears to prevail in the descending Pacific lithosphere (#7, 8, 9, 10). Strike slip with compression normal to strike of continental margin is also present (#16, 23). All lower hemisphere projections, compressional arrival quadrant shaded. Aseismic front: dotted line; Volcanic front: triangles; Alcalinevolcanism: star symbols.

4.6 Focal Mechanisms Study in the Eastern Aleutian Arc (L. House and K. Jacob)

The data analysis portion of the study of focal mechanisms for earthquakes in the Aleutian arc between 154°W and 176°W longitude has been completed. This task is a portion of a larger study using teleseismic data and published geologic and geophysical data to describe the subduction process in this 1500 km long arc segment.

Fault plane solutions fall in two categories: those of intermediate-depth events (>60 km) and those of shallow events (0 to 60 km). They are shown in map view in Figures 9 and 10, respectively.

The intermediate-depth events show predominantly downdip tension for events east of 165°W longitude and they belong generally to the group forming the lower zone of a weakly discernable double-planed seismic zone. West of 165°W many events with predominant downdip compression belong to the upper seismic zone, although a few other solutions do exist as well, some of which appear to belong to the lower seismic plane with preferred downdip tensional stress axes.

The shallow event solutions consist of regular thrust solutions associated with the main thrust zone and reflect the subduction of Pacific beneath the North American plate. Several normal faulting events are located at the trench reflecting bending of Pacific lithosphere as it approaches subduction. A few anomalous events show strong strike slip components with stresses consistent either with compression along the arc for those located within the downgoing plate, and with slip or fault orientations consistent with transverse

features cutting the arc for those events within the fore-arc region of the overriding plate.

A paper entitled "Earthquakes, Subduction, and Plate Deformation: Detailed Seismologic Observations in the Eastern Aleutian Arc", by House and Jacob (1982) is presently in its final stages of preparation.

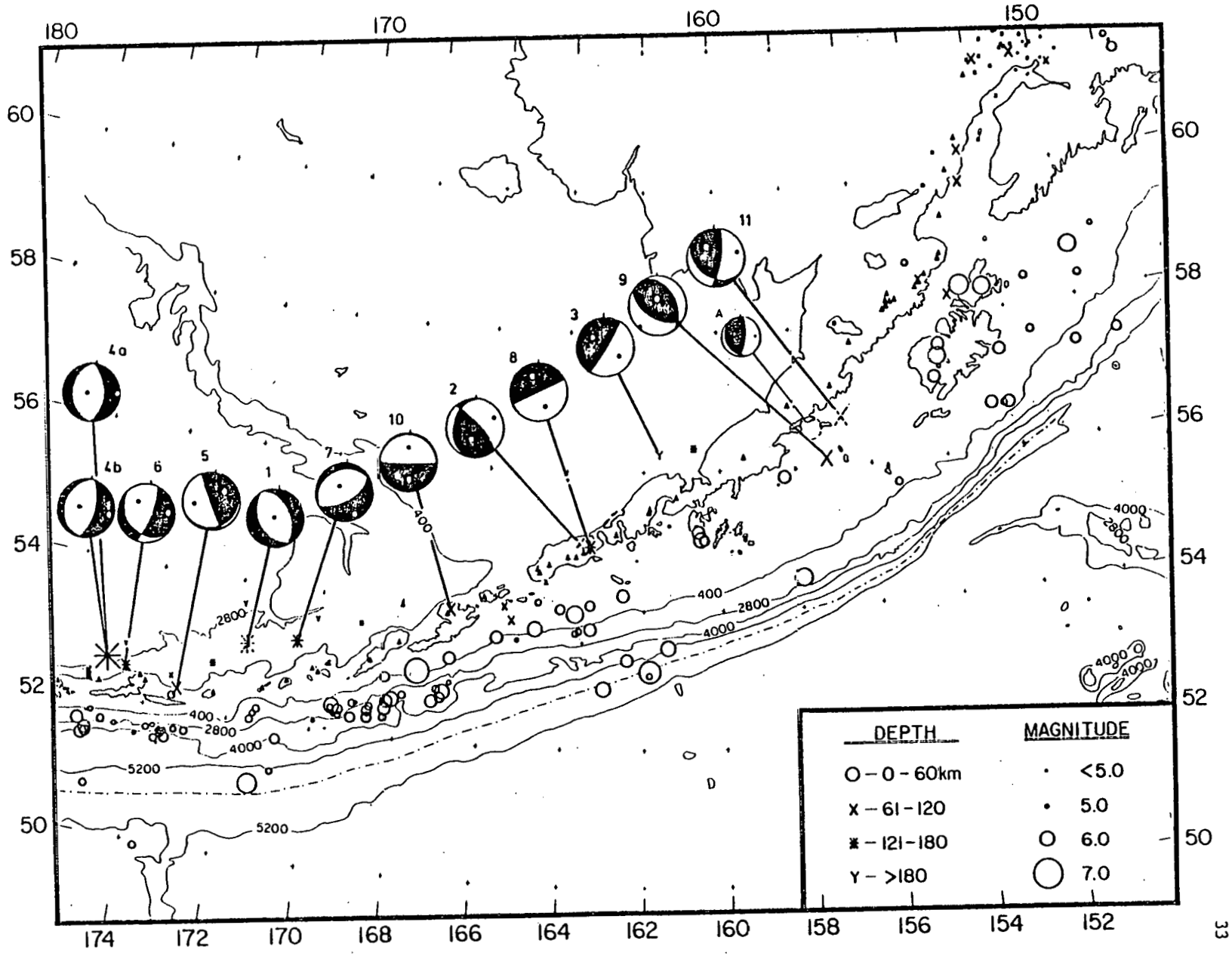

Figure 9. Map view of well-located intermediate-depth earthquakes and their newly determined focal mechanisms in the eastern Aleutian arc. Lower hemisphere projections with compressional quadrants shaded. Open dots are T axes, filled dots are P axes.

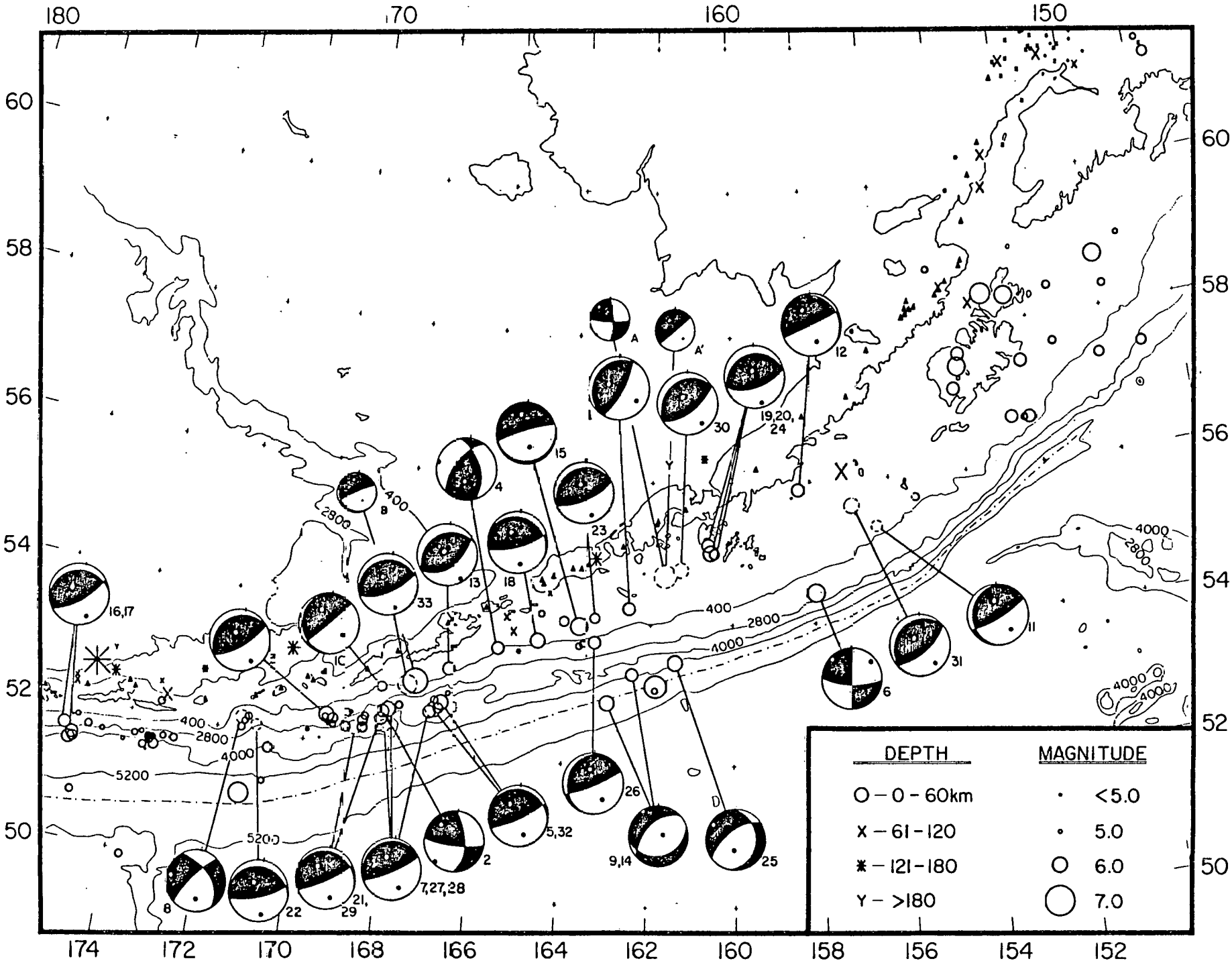

Figure 10. Map view of focal mechanisms of shallow earthquakes. Focal mechanisms are plotted as described in Figure 9.

4.7 A Mechanism for Formation of Summit Basins in Island Arcs (K. Jacob and L. House

During an ongoing detailed teleseismic investigation of subduction processes in the eastern Aleutian arc (House and Jacob, 1982) the following distinct tectonic features were recognized to closely coincide in space and time with the interaction of the Amlia Fracture Zone with the Aleutian trench and arc system (Figure 11):

1) A west-to-east decrease of the trench-volcano distance by about 40 km, resulting from a right lateral offset in the volcano line near Amlia Island (Figure 12).

2) A right-lateral offset also by about 40 km, of the intermediate-depth dipping seismic (Benioff) zone at about the same location at which the volcano line is offset (Figure 12).

3) Interruption of the 200-fathom bathymetric contour which elsewhere is continually outlining the high-lying features of the island arc (Figure 11). Thus, it indicates a local disruption (possible subsidence) of the present arc structure near Amlia Island.

4) Existence of at least two very recent arc-summit basins (the Amlia and Amukta basins) in the arc segment with the disrupted 200-fathom bathymetric contour. These two basins have a very young (<5M years?) and deep (several km) sedimentary fill (D. Scholl, T. Vallier, personal communication).

These features, together with the present position of the Amlia fracture zone and the present relative motion between the Pacific and North American plates of about 7 cm/year in a northwesterly direction

suggest to us the following possible process for arc summit basin formation (applying to at least these two basins): When a deep-seated bathymetric discontinuity in an oceanic plate, such as for instance associated with the Amlia fracture zone, passes obliquely or laterally beneath a subduction zone and associated arc, vertical readjustments take place within the overriding plate in the wake of the passage of the anomaly in the underriding plate. In this case the right lateral offset (either tear or warp) in the dipping Pacific plate causes a void-like structure in which either the overriding arc sinks directly, or into which upwelling fresh hot mantle material rises from beneath to fill the void. In either case the conditions are temporarily conducive to basin formation either by direct, primary subsidence of the arc or by rifting over a hot mantle diapir and secondary subsidence during cooling-induced contractional rifting. It is conceivable that the thermal history - and thus subsidence history - for these two mechanisms is distinct and if geologically recognizable - could be used to distinguish which of the two hypothesized processes may apply.

This finding, if confirmed by future field studies of fossil summit basins in now uplifted portions of island arcs, may have great bearing for predicting the existence of such summit basins within island arcs, where from marine geophysical studies passage of similar fracture zones can be inferred. Summit basins near volcanic arcs may have a moderate potential for hydrocarbon resources provided the appropriate sedimentation and thermal conditions prevailed for at least a few million years. So far arc-related basins have proven very erratic and unpredictable for exploration of oil or gas resources. In part this lack of predictability of their resource potentials may be

related to the presently poor understanding of their tectonic origins. Our working hypothesis is that at least a class of these summit basins is related to passage of offsets or of other bathymetric features in the descending oceanic plate. This hypothesis is testable by, however, only global comparison of tectonic settings of many of such basins. Several such Neogene basins appear to be present in the Alaska Peninsula, and are partly overprinted or covered by subsequent volcanism and related vertical tectonics (G. Bond, personal cummunication). The stratigraphy and (thermal?) subsidence history of these basins needs yet to be studied geologically. Our seismologic results (House and Jacob, 1982) using teleseismic data from the eastern Aleutian arc support the above presented hypothesis, but are insufficient to prove it.

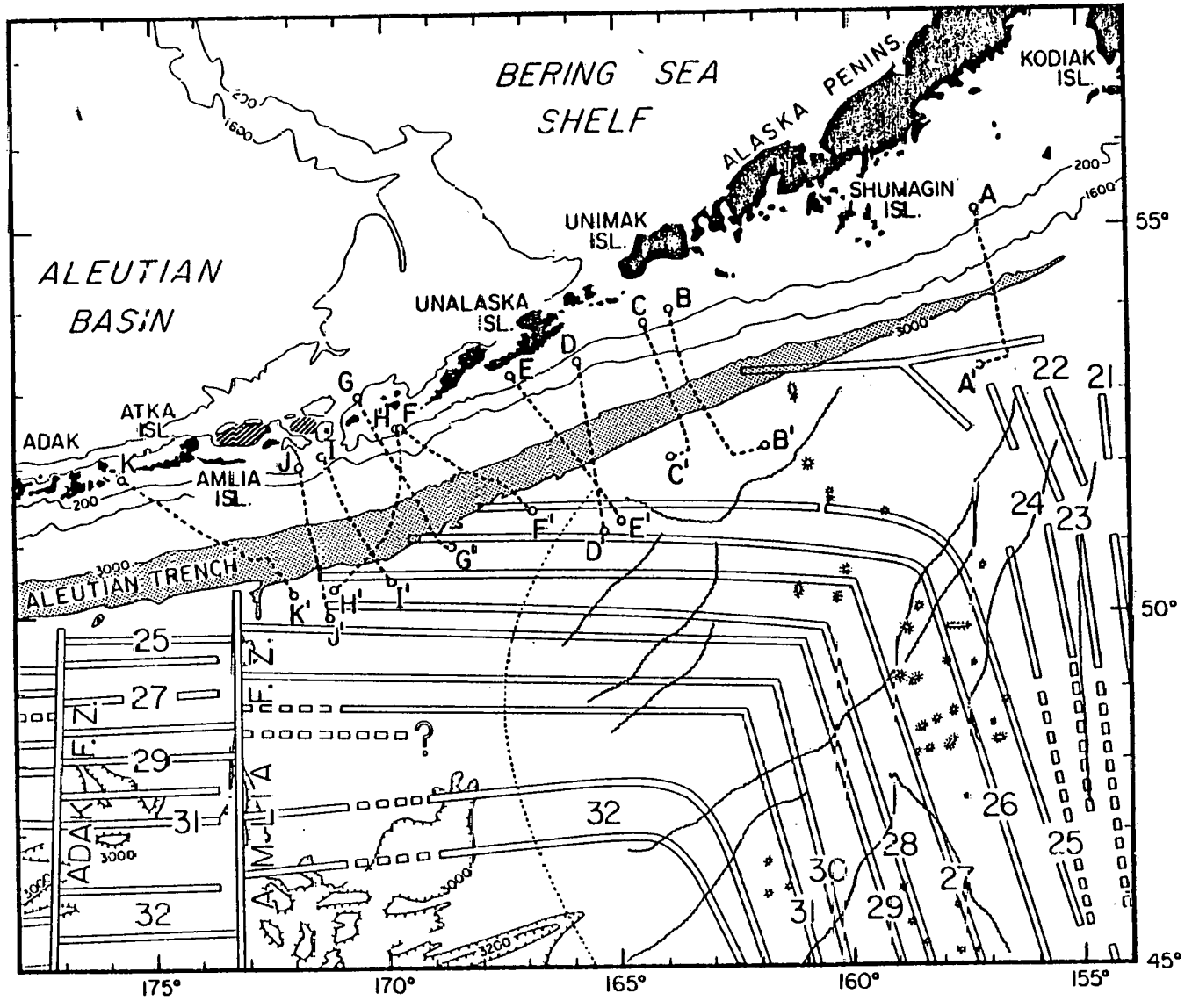

Figure 11. Map of eastern Aleutians with magnetic anomalies 21 through 32 plotted as series of double lines. Note the nearly 90° bend in the anomalies near 169°W (the Great Magnetic Bight). Anomaly 25 is 59 m.y. and anomaly 29 is 64.5 m.y. old; hence, crust to the east of Amlia Fracture Zone is about 5 m.y. older than comparable crust to the west. Fine dashed line outlines the extent of the turbidite fan of the Aleutian Abyssal Plain. Wiggly lines are extinct feeder channels for the turbidites. Angled shading denotes locations of summit basins within the island arc platform near 172°-173°W; Amlia Basin is farther west, Amukta Basin is to the east. Bathymetry is in fathoms (1 fm = 1.83 m).

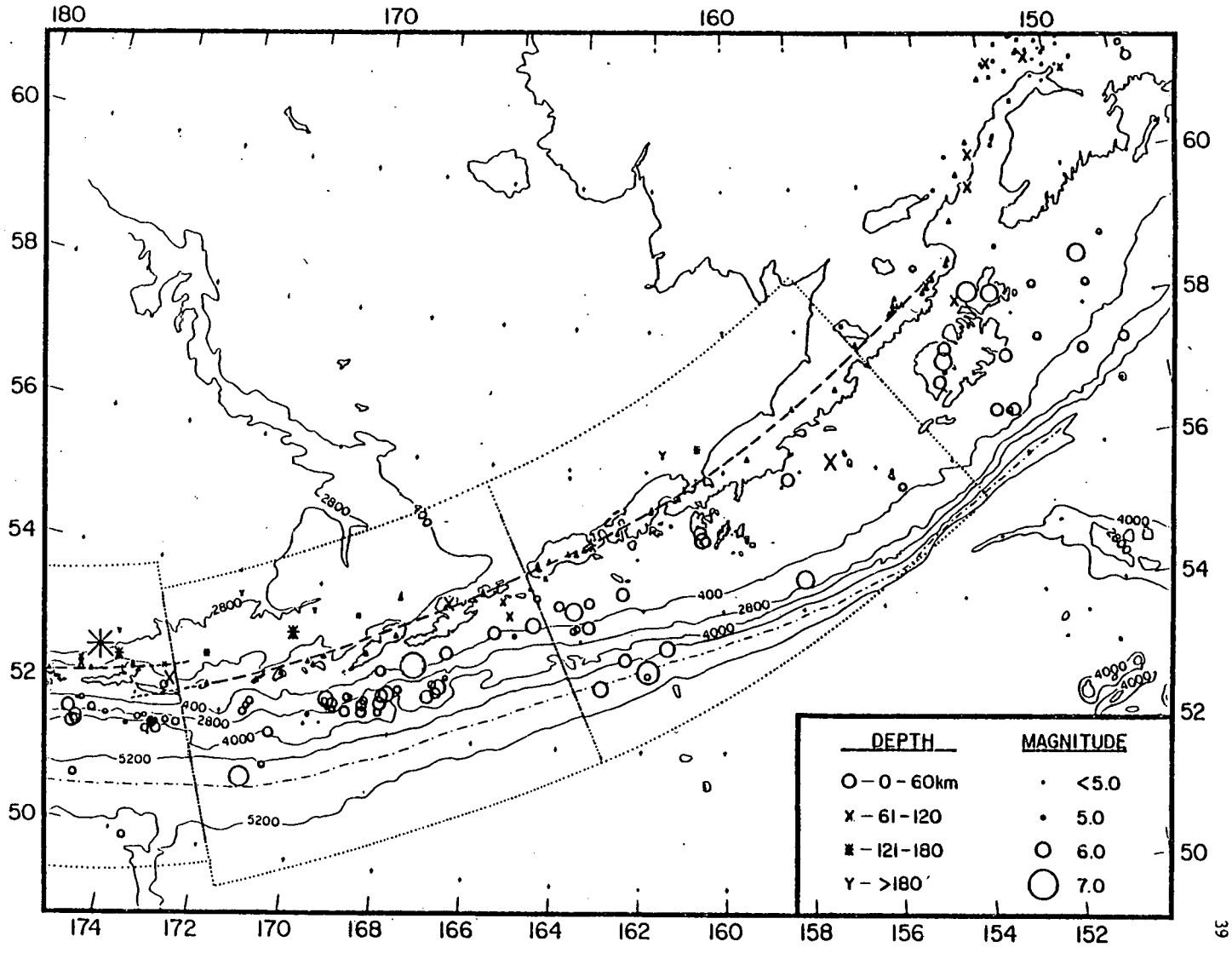

Figure 12. Epicentral plot of well-located earthquakes in the eastern Aleutians between 1965 and 1975. Symbol type and size are related to the depth and magnitude of the events, respectively. Solid triangles indicate locations of active volcanoes. The dashed line is a smooth curve through them, which is the reference for cross sectional views. Note the 40 km offset in the volcano line at about 173°W. Dotted lines define the boundaries of the three boxes used to produce cross sectional views: the western cross section extends to the left hand edge of the map, and is offset by about 40 km to the north. The dashed and dotted line indicates the axis of the Aleutian Trench.

4.8 Volcano Studies (S. McNutt)

Introduction

During the past year we have made progress in our Pavlof Volcano study on a number of observational areas, that raised several new research problems and possibilities. We are finally beginning to reap the benefits of our new upgraded recording systems, as new high quality data are being recorded on both analog and digital systems and as routine signal processing becomes more sophisticated.

To summarize, our study of seismicity at Pavlof volcano has progressed along several lines. Analysis of data from explosions is being used to shed light on the source and propagation parameters of b-type earthquakes, and to give information on the velocity structure of the upper part of the volcano. Harmonic tremor is being analyzed to determine its source characteristics and to infer length of a magma conduit where possible. Amplitude attenuation and time residuals of waves from regional earthquakes are being studied to delineate a low-velocity zone or possible magma chamber beneath the volcano. For the first time since initiation of the Pavlof study we obtained in the reporting period data of sufficiently high dynamic range and time resolution to tackle each of these 3 tasks. Thus, we are now developing and using several different tools of analysis to make the best use of these data for the study of the complex processes and structure of Pavlof Volcano.

Two major eruptions occurred at Pavlof during the past year. The first, on November 12-13, 1980, produced an ash cloud to 12,000 m

(37,000') and a lava flow approximately 3 km long on the north side of the mountain. The second eruption occurred on September 25-26, 1981, and occurred simultaneously with an eruption at Shishaldin Volcano 150 km to the SW (on Unimak Island). The September 25 Pavlof eruption produced an ash cloud to 10,000 m (33,000') and a lava flow approximately 3 km long on the NW side of the mountain. Both eruptions were accompanied by volcanic tremor and numerous b-type earthquakes (Minakami's 1960 classification of shallow events with emergent onsets, low frequency content, and lack of a clear S-phase). Additionally, a series of explosions were recorded during March and April 1981. Both eruptions were reported to the Smithsonian Institution Scientific Event Alert Network; the 1980 and 1981 eruption reports are included as Appendix 7.1. Dr. Egill Hauksson and Lazslo Skinta of Lamont were in the field less than one week after the September 25-26, 1981, eruption and were able to sample the fresh lava flow (still hot). The samples will be analyzed for major and minor element composition by Dr. Charles Langmuir of Lamont.

Signal Processing

During the past year we have concentrated on analyzing signals from volcanic explosions, harmonic tremor, and selected regional earthquakes. The shift to new data handling procedures has caused some of the initial analysis to be restricted to a small data volume, but the advantages of using the new high quality data are apparent even during preliminary work. Basically, an event large enough to be recorded on all Pavlof Network Stations (Figure 13) used to clip (go off scale) at nearer stations on film or paper records. The

new analog and digital magnetic tape systems have a higher dynamic range, and during playback and processing the traces can be easily separated, amplified, attenuated, stretched, compressed, and filtered. Figure 14 shows examples of explosions recorded during April 1981. We have chosen to examine first data from explosions for two reasons: 1) we know approximately where the explosions occur (at the summit crater), so we can use arrival time data and phase information as a kind of natural refraction experiment to deduce part of the velocity structure of the volcano; and 2) the seismic waves of explosions closely resemble the seismic waves of b-type earthquakes except for the air phase (see arrows in Figure 14). Studies of the waveforms of explosions will help us to identify phases, derive velocities and thus lay the basis to locate the b-type events – that is, we hope to find some similarities between the seismic waves of the two; since both have emergent onsets, any clear phase occurring later in the coda could be picked instead of the weak or emergent P-waves and used to locate the event, provided that such phases appear consistently. In Figure 14, one such phase appears fairly consistently on records from station PN7, and close similarities in the codas observed at other stations (possible phases) are also seen. The explosions at the summit crater may be preceded or are triggered by a slightly earlier seismic event within the volcanic pile, and may perhaps be caused by a pulse of magma injection.

So far we have had, however, little success in actually locating the pre-explosion events due to the emergence of arrivals. For understanding the physics of both magma injection and volcanic explosions it will be necessary to be able to constrain the locations

of the sources for both the b-type events and the pre-explosion events. Therefore we continue work on both of these problems.

Harmonic tremor, a roughly sinusoidal wave train of minutes to hours duration, has accompanied both of the recent Pavlof eruptions and many eruptions at other volcanoes as well (Kubotera, 1974). Often a gradual increase in tremor amplitude precedes the eruptions. We have begun an analysis of the frequency content of harmonic tremor from Pavlof, Fuego and Pacaya (Guatemala), Masaya and San Cristobal (Nicaragua) volcanoes using Fast Fourier Transform (FFT) and Berg Maximum Entropy spectral analyses methods. Preliminary results are quite encouraging; a sample of data is shown in Figure 15. A comparative study of data from several volcanoes may point to the common and variable processes that cause harmonic tremors in volcanoes. Our hypothesis here is that the frequency spectra represent eigenvalues of organpipe modes of vibration of magma in a conduit. If we can constrain the P-wave velocity of the magma in the pipe, then we can measure the length of the pipe from the frequency spectra and standard wave theory. We can also infer the boundary conditions from the overtone content of the spectra, hence possibly determine whether or not a shallow magma reservoir exists. Since two of the main unknowns here are the magnitude and homogeneity of the P-wave velocity in the magmapipe, we have also developed some software which will test for the frequency content of standing waves in an organpipe filled with variable velocity material, such as magma containing gas vesicles.

We have also advanced in our search for a magma chamber using amplitude attenuation and time residuals using regional earthquakes.

The data manipulating capabilities of our new software for seismic network analysis coupled with high quality data permit us to easily separate, amplify, and filter seismogram traces. This is particularly important for the magma chamber study, because to obtain useful and reliable results, it is necessary to obtain arrival time resolutions of better than 1/100 second for arrivals from earthquakes large enough to produce clean, impulsive arrivals. This new data handling capability ensures both high quality hypocenter locations and accurate measures of time residuals to stations of the Pavlof array. An earthquake large enough to give good data with the new recording systems would have clipped on our old recording system and made S-wave arrivals unreadable. Figure 16 shows an example of an especially clear and well-located earthquake. This particular earthquake is ideal for use in the magma chamber study since it occurred almost directly beneath the volcano (slightly northeast) at a depth of 172 km, hence its rays pass almost straight through the volcano's root zone from below. Table 2 shows the residual data from this event at the various Pavlof and other stations. We need to accumulate a sufficient number of recordings from similarly located events to 'X-ray' the volcano's root zone with sufficient spatial detail. We therefore abstain from an early interpretation of this data from a single sample event.

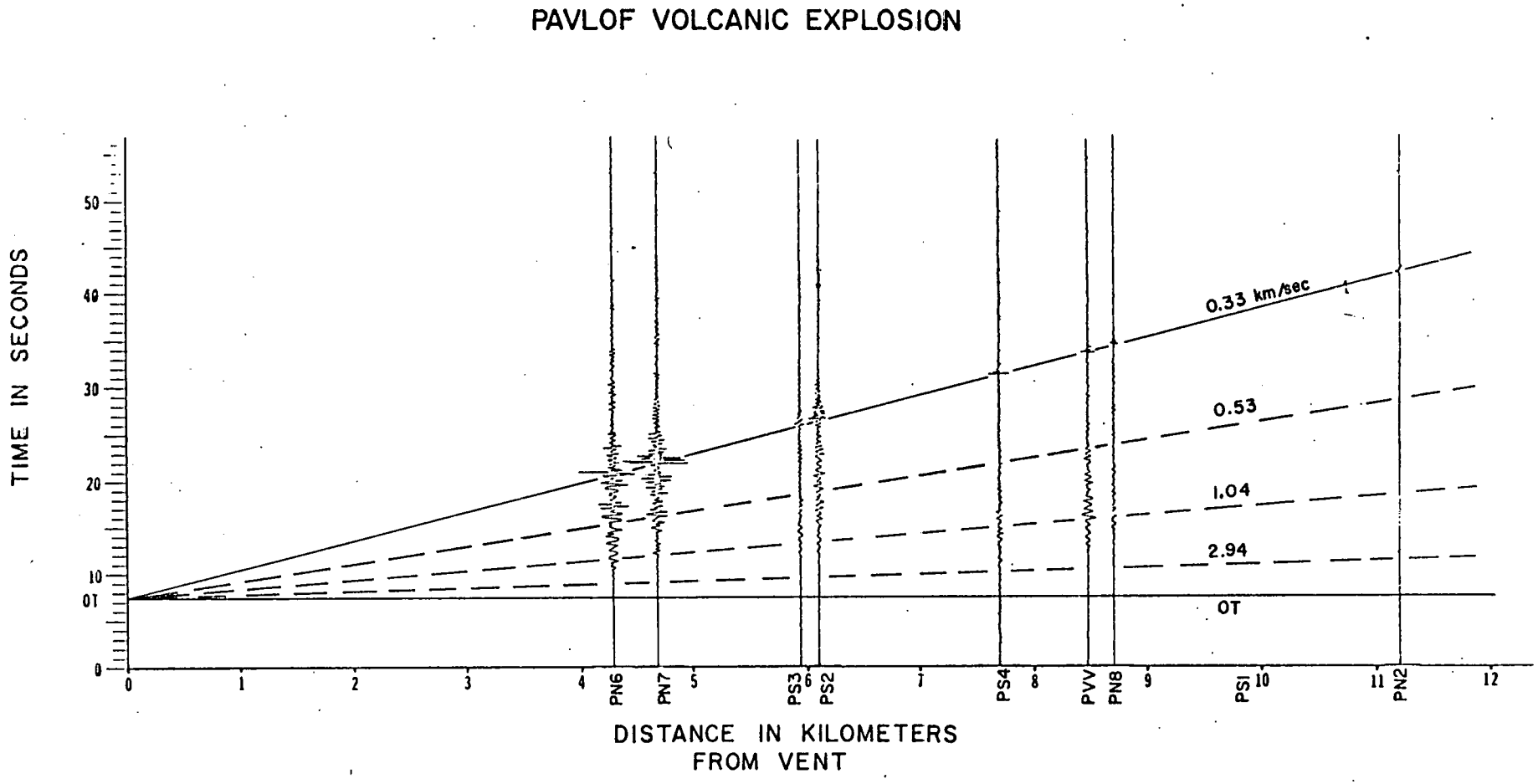

Figure 13. A volcanic explosion from Pavlof Volcano recorded at 8 stations of the Pavlof array. Note the impulsive air-wave arrival with a velocity of .33 km/sec. OT refers to the origin time as inferred from the air arrivals. The dashed lines are drawn to aid the eye in determining the velocities of other possible phases; they do not necessarily represent our final choice of phases. We note that the first emergent arrival at station PN6 has a velocity of 2.94 km/sec, a value consistent with P-wave velocities observed at other volcanoes.

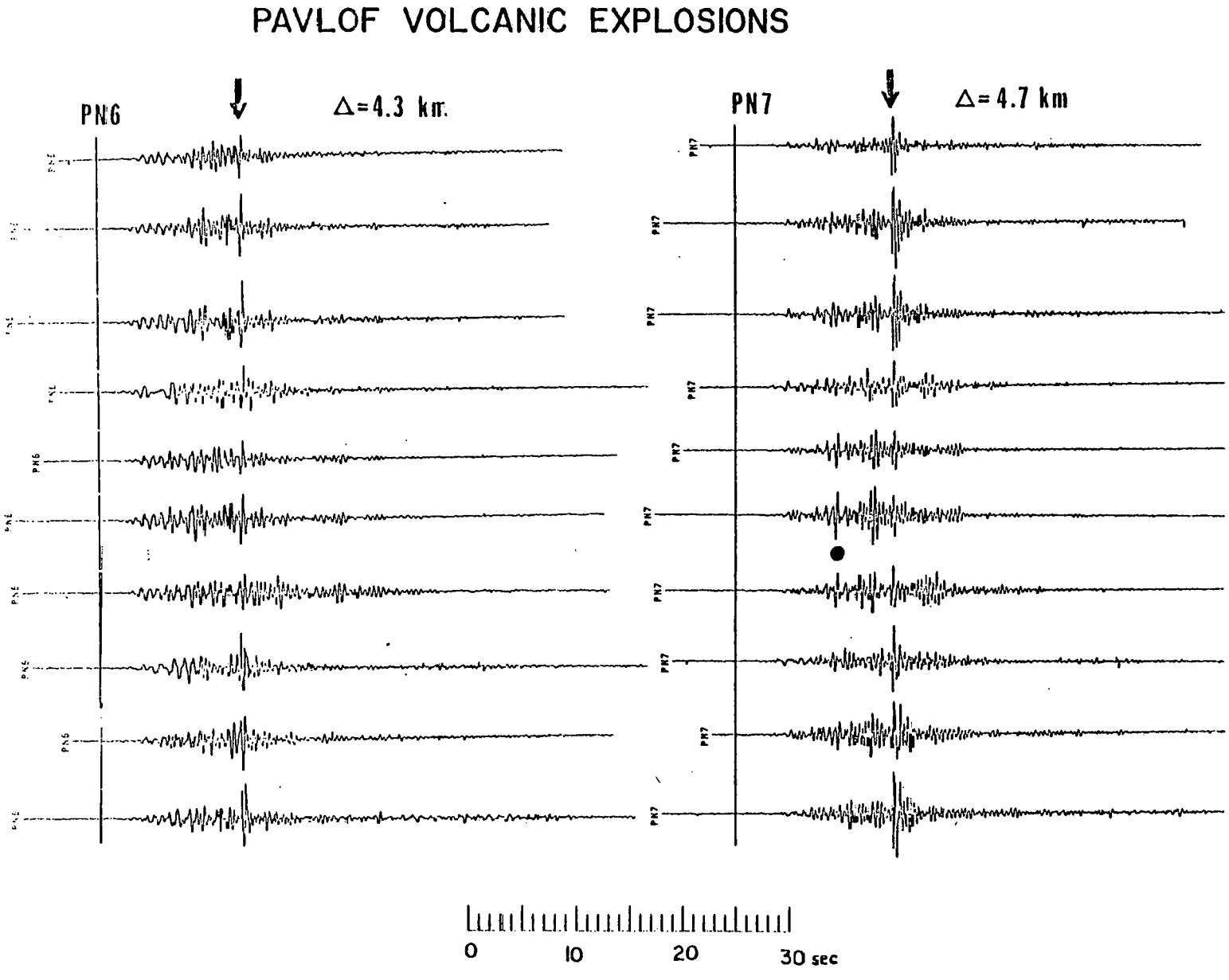

Figure 14. Ten different volcanic explosions as recorded at stations PN6 and PN7 are lined up according to the air-wave arrivals (shown by arrows). The vertical lines show the origin time. Note the distinct phase (velocity approximately 0.53 km/sec) indicated by the dot on station PN7.

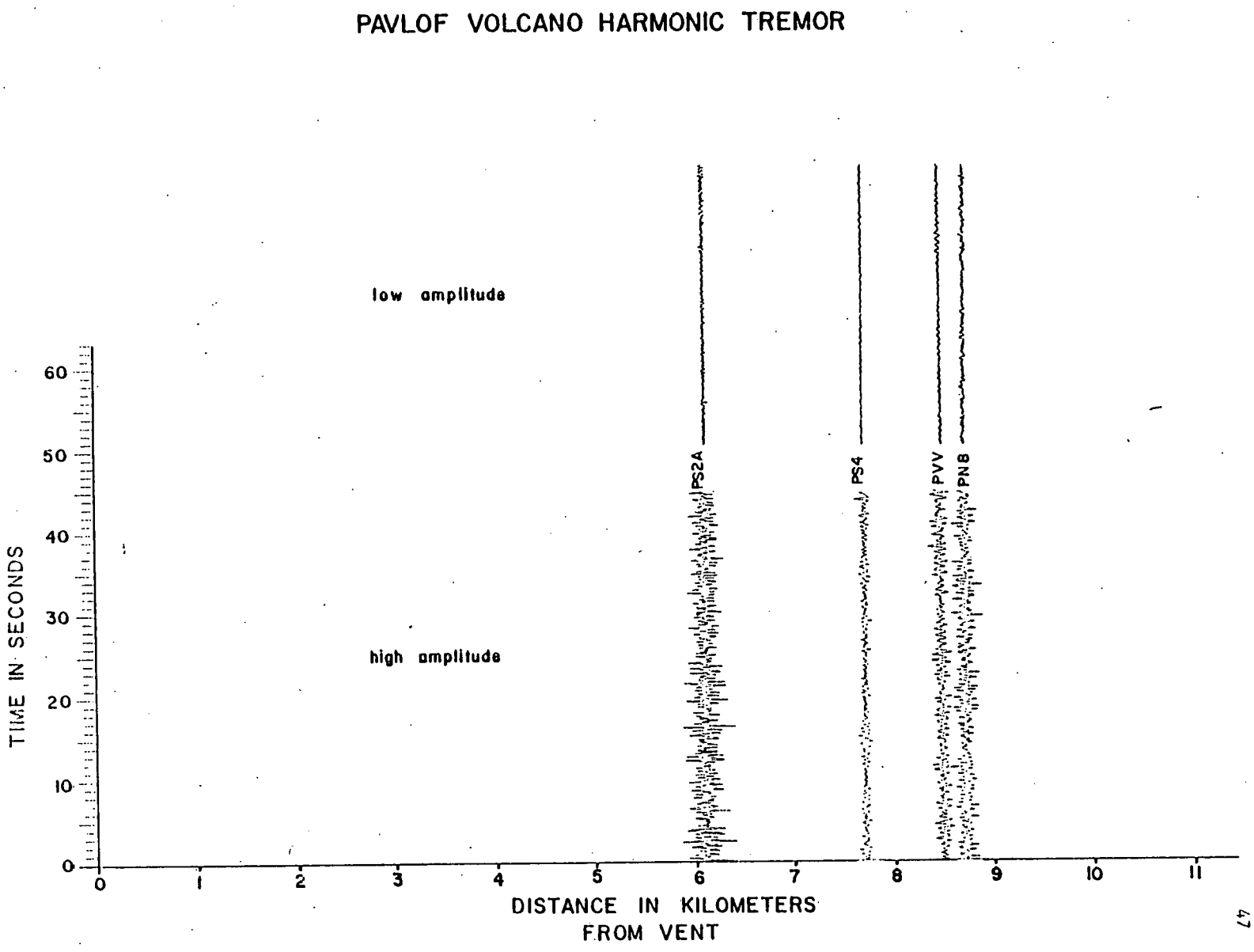

Figure 15. Harmonic tremor from Pavlof volcano as recorded at 4 stations of the Pavlof array. Traces are not corrected for magnification differences. Note the apparent higher frequency content of the signal recorded at station PS2A.

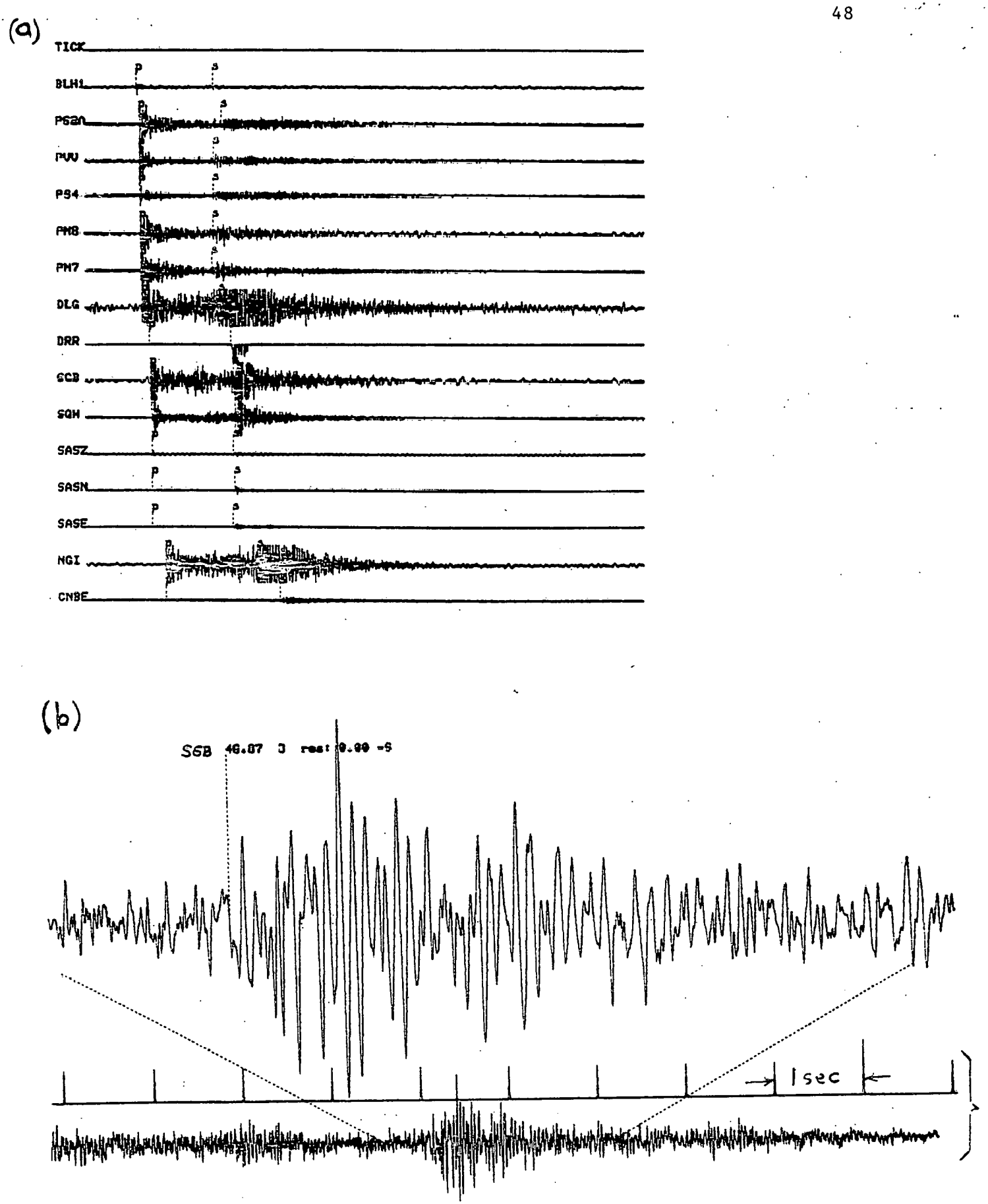

Figure 16. (a) Playback of seismic traces of event whose location and residuals are shown in Table 2. (b) Expanded playback of trace from station SGB showing improved resolution and our preliminary pick of the S-wave arrival time.

TABLE 2

Example of hypocenter location printout for event shown in Figure 16. This event occurred just northeast of Pavlof Volcano at a depth of 173 km. Note the two late-arriving P-waves at stations PN7 and PN8 (indicated by arrows).

yr mo dy	origin	lat n	lon w	depth	rms	erh	erz	gap	xmag	fmag
81- 8-19	2 8 3.39	55 36.38	161 53.53	173.33	.24	1.07	1.34	125		

rmswt	dmin	itr	nfm	nwr	nws	remk	q	sqd
.24	15.9	5	29	29	13		Ø	

sta	dist	azm	an	p/s	w	sec+ccor	(tobs	-tcal	-dly	=res)	wt	xmg	fmg	r	info
blh	15.9	312	174	ipu		25.55	.ØØ	22.15	22.57	.ØØ	-.41	1.49			.271
				es	4	42.55	.ØØ	39.16	39.Ø5	.ØØ	.12	.ØØ			.ØØØ
pn7	18.7	194	173	ipd	1	26.4Ø	.ØØ	23.Ø1	22.61	.ØØ	.4Ø	1.12		←	.Ø77
				es	3	42.27	.ØØ	38.88	39.12	.ØØ	-.23	.37			.Ø5Ø
pn8	2Ø.2	2Ø7	172	ipd	1	26.27	.ØØ	22.88	22.63	.ØØ	.25	1.12		←	.Ø63
				es	2	42.6Ø	.ØØ	39.21	39.15	.ØØ	.Ø6	.74			.2Ø6
ps2a	23.Ø	168	171	ipu	1	26.Ø6	.ØØ	22.67	22.67	.ØØ	.ØØ	1.12			.Ø62
				es	4	44.45	.ØØ	41.Ø6	39.22	.ØØ	1.84	.ØØ			.ØØØ
pvv	26.4	168	17Ø	ipd	1	26.Ø7	.ØØ	22.68	22.73	.ØØ	-.Ø5	1.12			.Ø58
				es	3	42.66	.ØØ	39.27	39.32	.ØØ	-.Ø5	.37			.Ø44
ps4	28.Ø	178	17Ø	ipd		26.17	.ØØ	22.78	22.77	.ØØ	.Ø1	1.49			.1Ø5
				es	3	42.62	.ØØ	39.23	39.39	.ØØ	-.16	.37			.Ø44
dlg	51.8	177	162	ipd		26.64	.ØØ	23.25	23.45	.ØØ	-.2Ø	1.49			.Ø81
				es	3	43.86	.ØØ	4Ø.47	4Ø.57	.ØØ	-.Ø9	.37			.Ø36
drr	8Ø.1	199	153	ep.		28.16	.ØØ	24.77	24.73	.ØØ	.Ø4	1.49			.123
				es	3	46.3Ø	.ØØ	42.91	42.78	.ØØ	.13	.37			.Ø34
sgb	89.6	94	151	ipd		28.39	.ØØ	25.ØØ	25.26	.ØØ	-.26	1.49			.111
				es	3	46.87	.ØØ	43.48	43.7Ø	.ØØ	-.22	.37			.Ø28
sasz	91.8	1Ø8	15Ø	ipd		28.61	.ØØ	25.22	25.39	.ØØ	-.17	1.49			.Ø95
				es	4	46.81	.ØØ	43.42	43.92	.ØØ	-.5Ø	.ØØ			.ØØØ
sqh	93.4	117	15Ø	ep.	1	28.58	.ØØ	25.19	25.49	.ØØ	-.3Ø	1.12			.Ø54
				es	2	47.22	.ØØ	43.83	44.1Ø	.ØØ	-.26	.74			.111
ngi	13Ø.5	118	14Ø	ipd		31.47	.ØØ	28.Ø8	28.Ø4	.ØØ	.Ø4	1.49			.185
				es	3	52.13	.ØØ	48.74	48.51	.ØØ	.23	.37			.Ø3Ø
snk	138.3	2Ø6	139	ep.		32.2Ø	.ØØ	28.89	28.65	.ØØ	.24	1.49			.261
				es		53.Ø6	.ØØ	49.67	49.56	.ØØ	.11	1.49			.593
ivf	15Ø.3	77	136	epu	2	33.32	.ØØ	29.93	29.63	.ØØ	.3Ø	.74			.Ø64
				es		55.13	.ØØ	51.74	51.26	.ØØ	.48	1.49			.435
bkj	154.7	1Ø8	135	ipd		33.55	.ØØ	3Ø.16	29.99	.ØØ	.17	1.49			.231
				es		55.Ø2	.ØØ	51.63	51.88	.ØØ	-.25	1.49			.451
cnbz	169.4	121	132	ep.	3	34.56	.ØØ	31.17	31.27	.ØØ	-.1Ø	.37			.Ø2Ø
				es	3	57.38	.ØØ	53.99	54.1Ø	.ØØ	-.1Ø	.37			.Ø41

4.9 Inhomogeneous Stress Release During Large Earthquakes (J. Mori)

Areas with an inhomogeneous stress field are likely to give rise to complex ruptures during large earthquakes. As the rupture progresses, subevents releasing high and low stress drop may occurr in the rupture zone. To look at these details in the rupture process the P wave for the March 28, 1964 Alaska earthquake was studied.

The first 120 seconds of the P wave as recorded on the Palisades broad band instrument are digitized and spectra are calculated for 10-second time windows using the Burg maximum entropy method. With a prediction filter length of 5 seconds the spectrum calculated with the Burg method is essentially the same as using a standard FFT, except the Burg method smoothes out the high frequency fall off. The results of the moving window analysis are presented in Figure 17. This figure shows a contoured plot of spectra for 12 time windows stacked on the vertical axis. All the spectra have been normalized at the low frequency end, so that high spectral amplitudes at high frequencies indicate a slower spectral fall-off with frequency. Note the peak in the 40-50 second time window. This peak shows that there is relatively more high frequency generated at this time interval in the signal than at other times. The fact that the high frequencies quickly drop off thereafter means that the effect is not due to multipathing or scattering which might cause high frequencies to arrive late. Also, this rapid drop-off is not simply a result of the earthquake having more moment at this time interval as demonstrated from Figure 18, which shows the signal being successively high-pass filtered to permit inspection at higher frequencies. Note that the

high frequency in the 40-50 second window does not correlate in time with the large amplitudes at lower frequencies that appear to arrive later. The arrival of the high frequency at 40-50 seconds corresponds to the largest subevent identified by Wyss and Brune (1967) in their analysis of the complexity of this earthquake. They were able to locate it reasonably well from its azimuthally varying arrival times relative to the first arrival which originated from rupture nucleation at the hypocenter.

The relatively high amounts of high frequency for this sub-event can be interpreted in several ways: 1) higher stress drop; 2) higher rupture velocity; 3) inhomogeneities in stress or material strength causing complex rupture; 4) locally high Q; and 5) break-out phase. All of the above except the break out phase indicate some change in material property or geometrical orientation. The suggestion that it is a material property is supported by looking at the aftershocks. All the larger aftershocks that were well recorded on the Palisades instrument are shown in Figure 19. As in the moving window analysis, contoured spectra are shown except instead of time windows, the various aftershocks are stacked on the vertical axis. Only the first few seconds of the P wave were used in order to avoid contamination from depth phases.

Although the distribution of aftershocks does not adequately cover the rupture area, differences can be seen in the spectral content of earthquakes in the regions where there are large aftershocks. Note the high frequency content for event 6, which can also be seen in the seismogram itself. The location of this aftershock is quite close to the location of "subevent C". So it

appears that this area generates relatively large amounts of high frequency when ruptured by an earthquake.

An observation which suggests that this high frequency is due to inhomogeneities (i.e., local areas of high stress or strength) comes from a comparison of aftershocks 6 and 3. Note that the pulse shapes are similar but event 6 has the high frequencies riding on top of the lower-frequency pulse shape. This pulse form is interpreted as indicating a complicated rupture with many small subevents which have high dynamic stress drops. This complexity suggests further that the close proximity of high and low stress drop earthquakes may be indicative of an area of inhomogeneities on the order of a few kilometers. Such regions would be expected to produce relatively great amounts of high-frequency radiation and thus higher ground accelerations during rupture in a large earthquake; thus, the existence of heterogeneities on the rupture plane may control how much potential damage the earthquake is capable to cause.

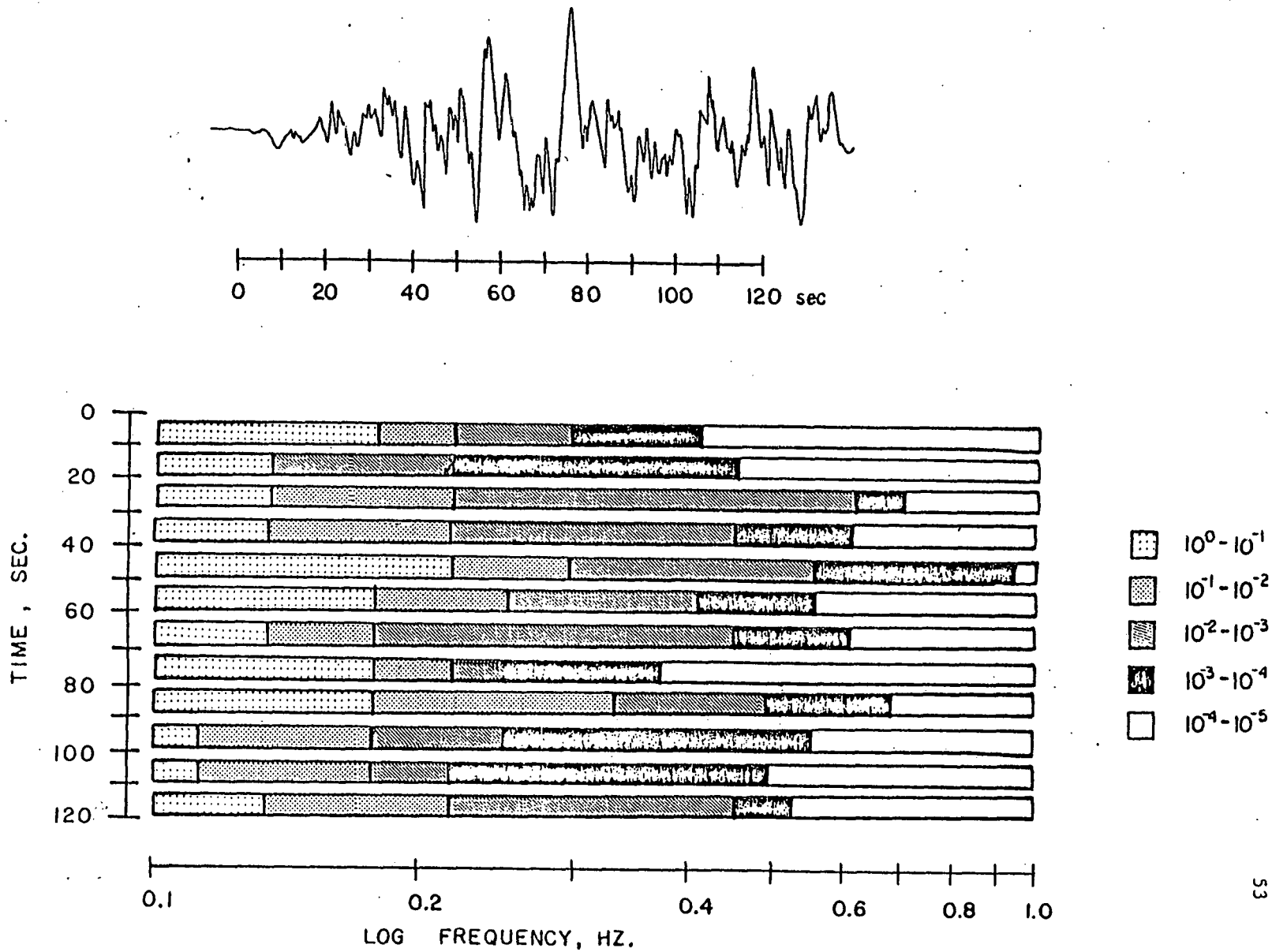

Figure 17. Moving window analysis of P wave recorded at Palisades for 1964 Alaska earthquake. Contoured spectra for each time window are stacked on vertical axis. Spectra have been normalized to the low frequency (0.1 Hz) value. Note the relatively large amounts of high frequency in 40-50 second time window.

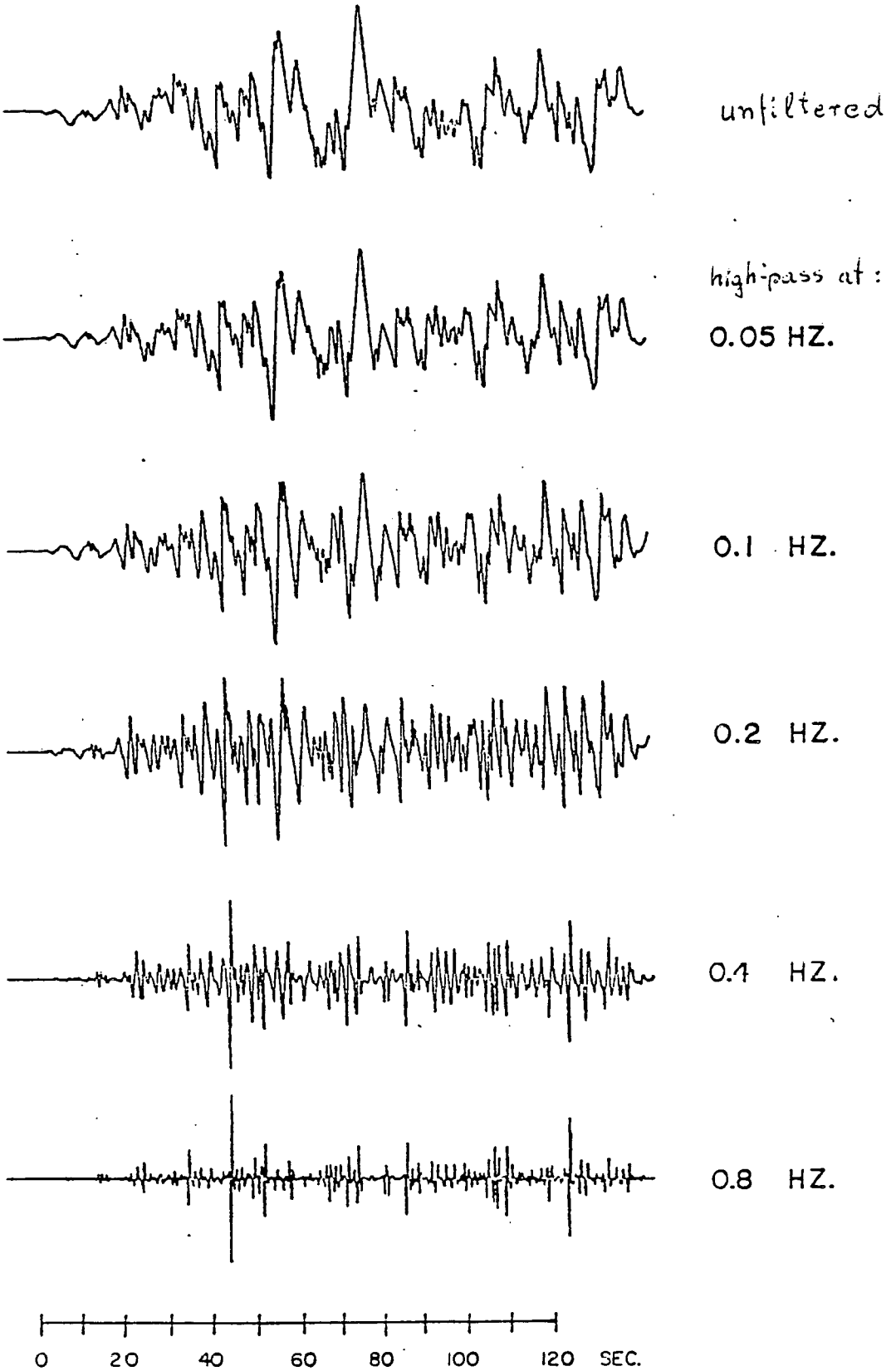

Figure 18. P wave of 1964 Alaska earthquake successively high pass filtered. Number on right is 3db point of Butterworth high pass. Note that the large amount of high frequency in the 40-50 second time window does not correlate with large amounts of lower frequency radiation.

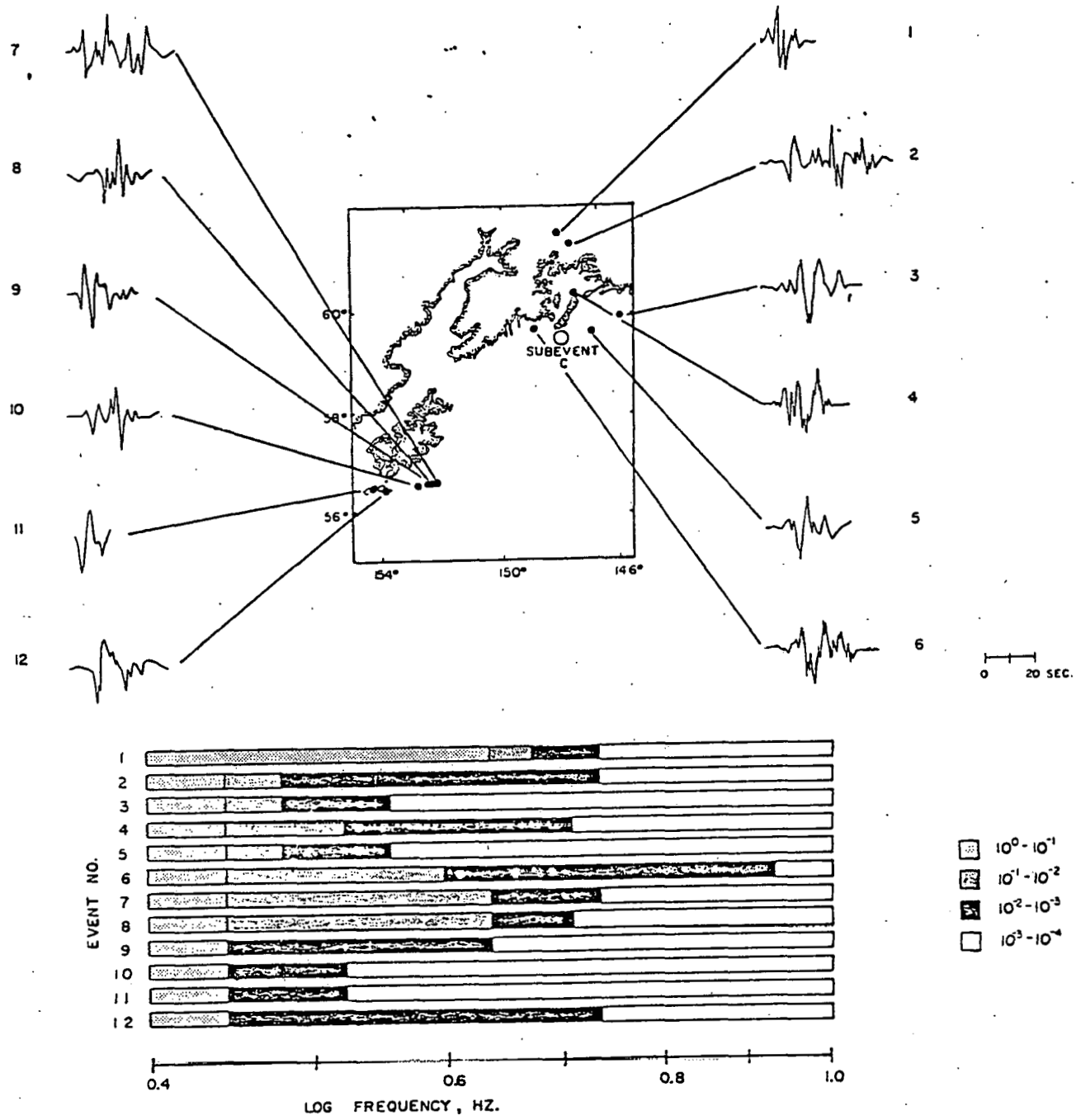

Figure 19. Spectral analysis of aftershocks of 1964 Alaska earthquake. Contoured spectra for each aftershock are stacked on vertical axis. Aftershock 6 generates relatively more high frequencies, as seen in its spectrum and seismogram.

4.10 Magnitude Determinations (J. Peterson and E. Hauksson)

Objectives. One of the purposes of operating the seismic network is to determine the magnitude of local earthquakes. Either the body wave magnitude or the coda length magnitude for local events can be determined. A body wave magnitude is a more useful measure of the size of a local earthquake since it represents the measured ground motion at the respective seismic station. The coda length magnitude can be more easily determined since no calibrations of the instruments are needed as long as they remain unchanged. The coda length magnitude, however, is not a known function of ground motion and is sometimes dependent on the S-P-arrival time of the local earthquake. Prior to 1980 we determined coda length magnitudes for earthquakes that occurred within our network. Since much of our instrumentation was upgraded in 1980 and 1981 we were faced with the task of redetermining our coda length magnitude scale or to calibrate our instrumentation to facilitate the calculation of body wave magnitudes. We decided to calibrate our instrumentation since that permitted us to use the network to achieve other scientific goals (for example, attenuation studies, calculation of source parameters) in addition to enabling us to determine body wave magnitudes.

The calibration of the seismic network was carried out in two different ways. First, all individual components were calibrated in the laboratorium or specifications on instrument characteristics were obtained from the respective manufacturer. This information (see Figure 20) was combined into a total system response as described below to determine ground motion in nanometers (nm, 10^{-9} m). Second,

the seismic stations were calibrated in the field during the October 1981 field trip. A constant-current-square-wave signal of 10 second period was applied to the calibration coil of the seismometer. These calibration pulses can be used to confirm the results obtained using the first method. Further, at 10 seismic stations in the network a calibration signal is generated automatically every 24 hours to check if the station's calibration changes with time. The calibration data from the October 1981 field trip is currently being analyzed.

Calculation of the Total System Response. The total seismograph system response, TSS(f) at frequency, f, is the product of the sensor response SR(f) and recorder response RR(f) (see Figure 20).

$$TSS(f) = SR(f) \times RR(f)$$

The sensor response, SR(f), is the product of the seismometer response, S(f), and the amplifier response, A(f), or

$$SR(f) = S(f) \times A(f)$$

The seismometer response as a function of frequency was calculated with the following formula:

$$S(f) = \frac{2\pi f^3 G_E}{[(F_o^2 - f^2)^2 + 4B_t^2 F_o^2 f^2]^{1/2}} \qquad [V/mm]$$

where G_E is the effective motor constant [V/mm/sec]

F_o is the natural frequency [Hz]

B_t is the damping ratio (parallel or series)

The amplifier response vs. frequency (A(f)) was measured during a calibration sequence in the laboratorium. This is a relative function that is normalized to 1.0 on the flat portion of its response curve. The sensor response is normalized to a 42 db attenuation of the station amplifier VCO (i.e., gain 90 db, attenuation 42 db) since that is a commonly used value in our network.

Further, the sensor response is normalized to 1.0 at 2.51 Hz for numerical convenience. The actual value of SR (2.51) constitutes the sensor gain G^S, or

$$SR(2.51) = G^S$$

The recorder response function, RR(f) is the product of telemetry gain, T(f) and recording device sensitivity, R(f).

$$RR(f) = T(f) * R(f)$$

The telemetry gain is always set equal to one. The recorder sensitivity is determined by the particular input filters that were calibrated in the laboratorium. The recorder response is normalized at 2.51 Hz and the actual value of RR(2.51) constitutes the recorder gain, G^R.

Therefore, the normalized seismogram system response is determined by the SR(f) and RR(f) as shown in Figure 20. To obtain

the total system response these curves have to be multiplied by the sensor gain, G^S and recorder gain G^R. If the VCO attenuation setting differs from -42dB it is taken into account when calculating G^S.

Conversion of Recorded Amplitudes to True Ground Motion. A program was developed to filter the phase data and convert the measured amplitudes to ground motion in nanometers. The appropriate TSS functions are stored for the seismometer, VCO, recorder combinations that are listed below. Also stored are the total gain factors for each TSS and an attenuation look-up file for handling the VCO attenuation setting variability, extra damping pads and exceptional VCO units (e.g., 114 db as opposed to the regular 90 db units).

Geophones

Mark L4-C, 1B
Geospace HS-10 (3 main coil resistances, 3 external dampings)
Norsar HS-10
Broad Band (Baby Benioff) SP, IP

Amplifiers-VCO's

Emtel 6242 (90 db, 114 db)
Develco 6202 (90 db)

Recorders

Develocorder
TEAC analog to digital
Digital system (ADC gain 1, 2)
Helicorder
Crown analog tape
Sangamo analog tape

True ground motion is simply the recorded amplitude divided by the product of the total seismograph system response, total gain and attenuation factors.

Calculation of Earthquake Magnitude. To determine the local magnitude scale such that it is calibrated with respect to the body wave magnitude, M_B, published in monthly PDE bulletins, the following approach is taken:

From Richter (1958) we have for a Wood-Anderson instrument

$$M_L = \log A - \log A_o$$

where A is the zero to peak of the largest phase on the record in mm and A_o is a distance correction. When correcting for the gain of the W-A we obtain

$$M_L = \log (A/2800) - \log A_o + \log 2800$$

$$M_L = \log (A_q) - 0 + \log 2800 - \log A_o$$

where A_q is measured ground motion in mm. Instead of measuring the largest phase on the record which in our case is most often a surface wave or an S-wave, we measure the largest amplitude in the P-wave train. This permits us to determine a local body wave magnitude as

$$M_b = \log A_{pq} - 2.55 - \log A_o.$$

We prefer to use the largest P-wave amplitude (A_{pq}) since it is less often saturated or clipped than the S- or surface wave amplitudes.

Each event and each station magnitude, M_b, is then compared to the PDE M_B and a systematic difference of C = 0.8 = M_B-M_b was found. We then checked the dependence of the difference of the two, C = M_B-M_b, on distance, depth, magnitude and individual station but no obvious relationship was found. A constant value for C = 0.8 is then added to make our local bodywave magnitude compatible to the PDE body wave magnitude. Hence our reported body-wave magnitude M_B (as shown in cols. 73-75 in data files submitted to NOAA) is determined by the formula

$$M_B = \log A_{pq} - 1.35 - \log A_o(\Delta)$$

In the future we plan to attempt a comparison to Palmer reported magnitudes for the greater Shumagin region.

Coda length magnitude. In rare cases we still report coda length magnitudes when a body wave magnitude cannot be determined. The surface wave magnitude, i.e., coda length magnitude, reported (as shown in cols. 61-63 in data files submitted to NOAA) are determined using the FMAG formulation of J.C. Lahr (1980) and his empirical constants derived for Alaska.

$$FMAG = C_1 + C_2 \log (F_\gamma) + C_3\Delta + C_4 Z + C_5 (\log (F_\gamma))^2$$

$C_1 = -1.15$ $C_3 = 0.0035$ $C_5 = 0.0$

$C_2 = 2.0$ $C_4 = 0.007$

C_5 may be determined in the future with a larger data set "to compensate for the nonlinear relationship of log (coda) and magnitude."

F = F-P time; measured from P onset to 1 cm p-p amplitude cut-off

Δ = epicentral distance (km)

Z = hypocentral depth (km)

γ = station correction (1 used here)

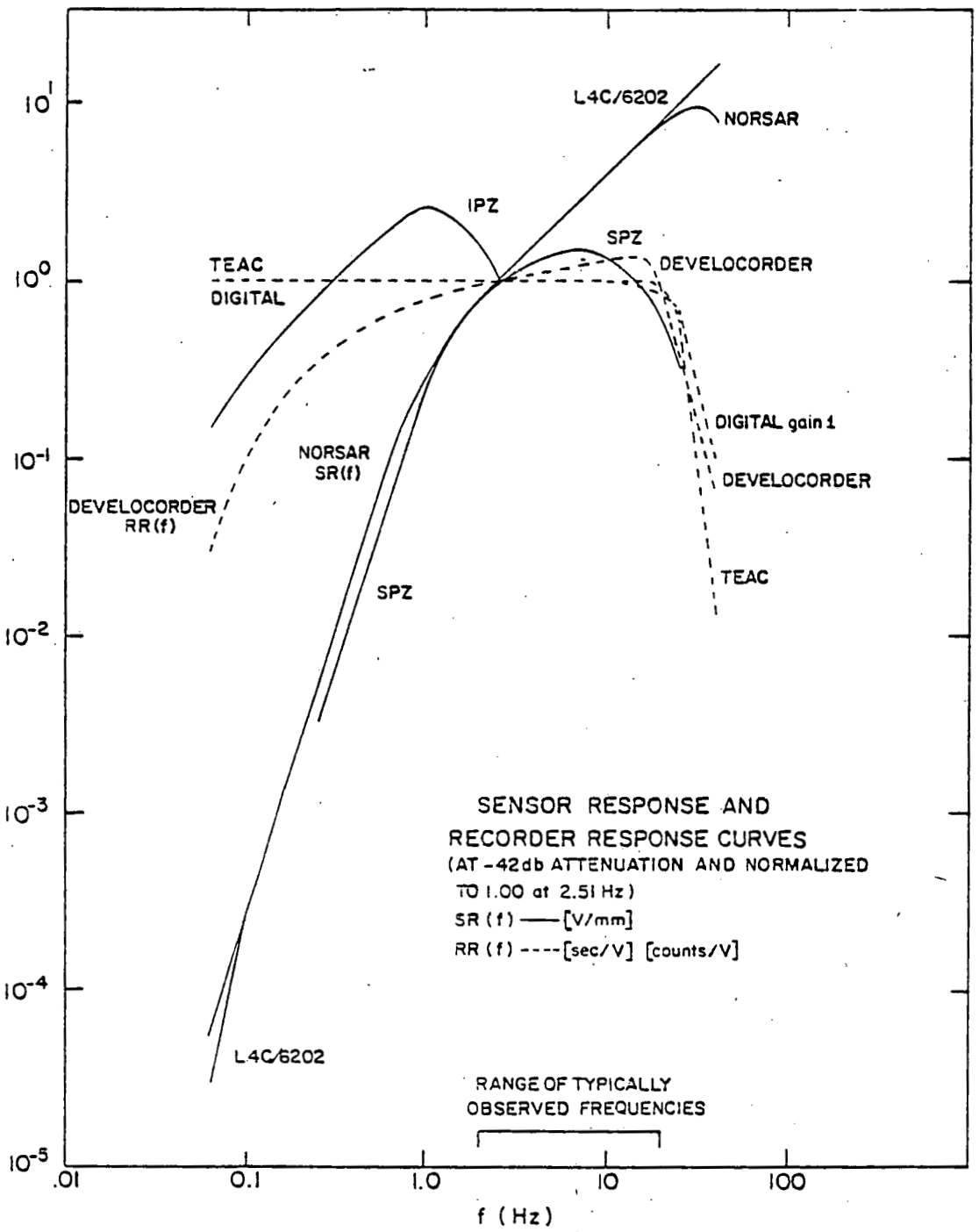

Figure 20. Sensor responses and recorder responses shown as a function of frequency for seismic stations in the Shumagin Network. The sensors are short period vertical (SPZ) and intermediate period vertical (IPZ). The SPZ sensors are either NORSAR HS-10 or Mark L4-C/6202, 1B seismometers. The IPZ sensors are broad band (Baby Benioff) seismometers. The recorders are continuous recording on a film (DEVELOCORDER), an event triggered analog tape recorder (TEAC) and an event triggered digital tape recorder (DIGITAL). Above the horizontal axis the range of typically observed frequencies is shown. The sensor and the recorder responses are combined to get the total system response as described in the text.

5. TECHNICAL ACCOMPLISHMENTS

5.1 Network Status, October 1981 (following summer fieldwork)

There are now only two networks operated by L-DGO is the eastern Aleutian arc, the Unalaska Network (Figure 21), recorded at Dutch Harbor (DUT); and the Shumagin Network (Figure 22), recorded at Sand Point (SAN).

This summer (1981) the Pribilof Network was deactivated because the current NOAA/BLM OCSEAP funding is not sufficient to continue operating the network. Initially, the Pribilof and Unalaska Networks were established with the support of NOAA.

The Shumagin network and its subarray on Pavlof Volcano was establishd largely with support from the DOE and some initial equipment from the USGS. The original purpose of the Shumagin Network was to provide data for tectonic studies with some geothermal studies being added when the Pavlof subarray was installed. The data from all of these networks can, of course, be used for both hazards and tectonic studies; indeed, there is a synergistic benefit in carrying out these studies simultaneously.

5.2 Unalaska Network

Remote stations. The network (Figure 21) consists of four remote seismic stations and one repeater station. One new station (USR) was installed during summer 1981. The seismometers at the remote stations are all short-period (1 Hz) vertical instruments and the data are

transmitted via VHF-links to the central recording station at Dutch Harbor (DUT).

Central recording station. The sensors at the local station (DUT) consist of three orthogonal short-period seismometers, an intermediate-period (≈15 sec) vertical seismometer and an orthogonal set of strong motion accelerometers. The data acquisition system consists of an event-triggered TEAC audio tape recorder and two continuously operating helicorders. A Universal time receiver for the standard time broadcast via satellite provides a stable time standard.

Future outlook. The NOAA/BLM OCSEAP funding will be terminated by the end of September 1982. Currently we are investigating the possibility of alternative funding related to a geothermal project on Unalaska Island. If we do obtain alternate funds, we will continue operating the Unalaska Network. If we are unable to find a new funding source, we plan to deactivate the network. Some of the instrumentation will be stored on site until new funds become available to reactivate and continue the operation of the network. Some of the hardware will be used in the Shumagin network if the Unalaska network is going to be terminated.

5.3 Shumagin Network

Remote stations. The Shumagin Network (Figure 22) consists of 13 remote stations plus 8 stations in the Pavlof Volcano subarray, three repeater stations and the local station at Sand Point (SAN). Each remote station has a single, short-period vertical seismometer except San Diego Bay (SGB) and Chernabura (CNB) which are now three-component

stations. Within the region of the Shumagin Network there are now twelve strong-motion accelerographs (SMA) ten of which are co-located with remote stations of the network (Figure 22). Further, these ten SMA's are connected to the telemetry system so that a trigger signal allows us to know the exact time at which the SMA began recording a given earthquake. Most of the support for these SMA instruments came from a USGS contract. This system has already been triggered several times by local events.

Central recording station. Sensors local to the recording center at Sand Point (SAN) consist of orthogonal sets of short-and intermediate-period seismometer, and strong-motion accelerometers.

Eight helicorders that record continuously and two event-detecting, magnetic tape recording systems (one analog and one digital) are operated at Sand Point. The analog event-detector consists of one to eight signal-detector modules and a logic unit which is based on a programmable-read-only-memory (PROM) chip. The signal-detectors switch to an "on" state whenever the short-term average (STA) of the signal exceeds the long-term average (LTA) by some selectable level. The PROM can be programmed so that any logical combination of states of the signal-detectors can cause the event-detector to declare an event and switch on the tape recorder. Two four-channel TEAC audio tape analog recorders are used: one in a continuous-loop mode to provide a twenty second pre-event "memory", and the other in a standard, reel-to-reel mode to record the data. Frequency-modulated tones from the remote and local sensors are mixed onto the four channels along with an IRIG time code from a satellite-controlled clock and a frequency-compensation tone. Eight

to ten signals can be mixed onto three of the channels and five can be mixed with the 1000 Hz time code, so that a total of about 32 signals can be recorded. In addition to the tones from the seismic stations, 400 Hz tones from the SMA trigger units are also recorded. Whenever one of these tones is detected the tape recorder is always turned on, so that the on- and off-times of the SMA's can be determined. The magnetic tapes are demodulated, digitized and processed at L-DGO.

At Sand Point we have installed an uniterruptible power-supply (UPS) system that consists of a short term battery back-up unit and a long term propane powered alternator. The battery-backup is designed to provide 4 to 8 hours of uninterrupted power for the entire station should the town power system fail. The propane powered alternator units are designed to automatically start after about 80% of the battery capacity has been used and to run for about one week without refueling.

In December 1980 a new digital recording system was installed at Sand Point. The seismic signals are digitized at a rate of 100 samples per second and up to 32 channels can be recorded on the computer compatible nine-track tape. This data acquisition system was developed and built by the L-DGO seismology engineering group. Currently, in October 1981 a new 12 channel digital event detector is being installed in Sand Point and interfaced with the digital data acquisition system. The digital event detector can be accessed from L-DGO via the L-DGO seismology computer through modems. Further, in October 1981 all the equipment at the central recording station was moved into a new room from an adjacent smaller room, within the same building. When the new data acquisition system was installed it

became clear that previous failures caused by excessive dust and poor ventilation could only be eliminated by relocating the equipment, and providing new adequate ventilation.

5.4 Future Outlook

During the next field season (summer of 1982) we plan the following changes in the Shumagin network:

1. The four repeater stations, CHR, ZKB, SQH, and SGR will be combined into one repeater station located on Popof Island. This new repeater will be located at a highpoint accessible on land from Sand Point and thus will save considerable Helicopter costs.
2. The stations, NGI and BKj have to be relocated to facilitate transmission of signals via the new repeater.
3. The stations, SQH, PS2A and PS3 will be discontinued.
4. The stations, BKJ, IVF and PVV will be upgraded to three component stations.
5. All stations will be serviced such that they will last for two years as opposed to the present one year lifetime. At some stations we will deploy a double set of batteries and at other stations we plan to install panels of solar cells and rechargeable batteries.
6. A digital transmission link will be installed between SGB and Sand Point.

During the past years helicopter support was provided by the NOAA/BLM OCSEAP program. We have now been informed that the summer of

1982 will definitely be the last year of NOAA helicopter support. This support would cost about $100,000 from a private contractor and is vital to the maintenance of the networks. We plan to find alternate sources of funds and will make an effort to make the network more easily serviced. As listed above, we plan to combine repeater stations and to service the remote stations every other year. These efforts could possible half our helicopter costs in the future.

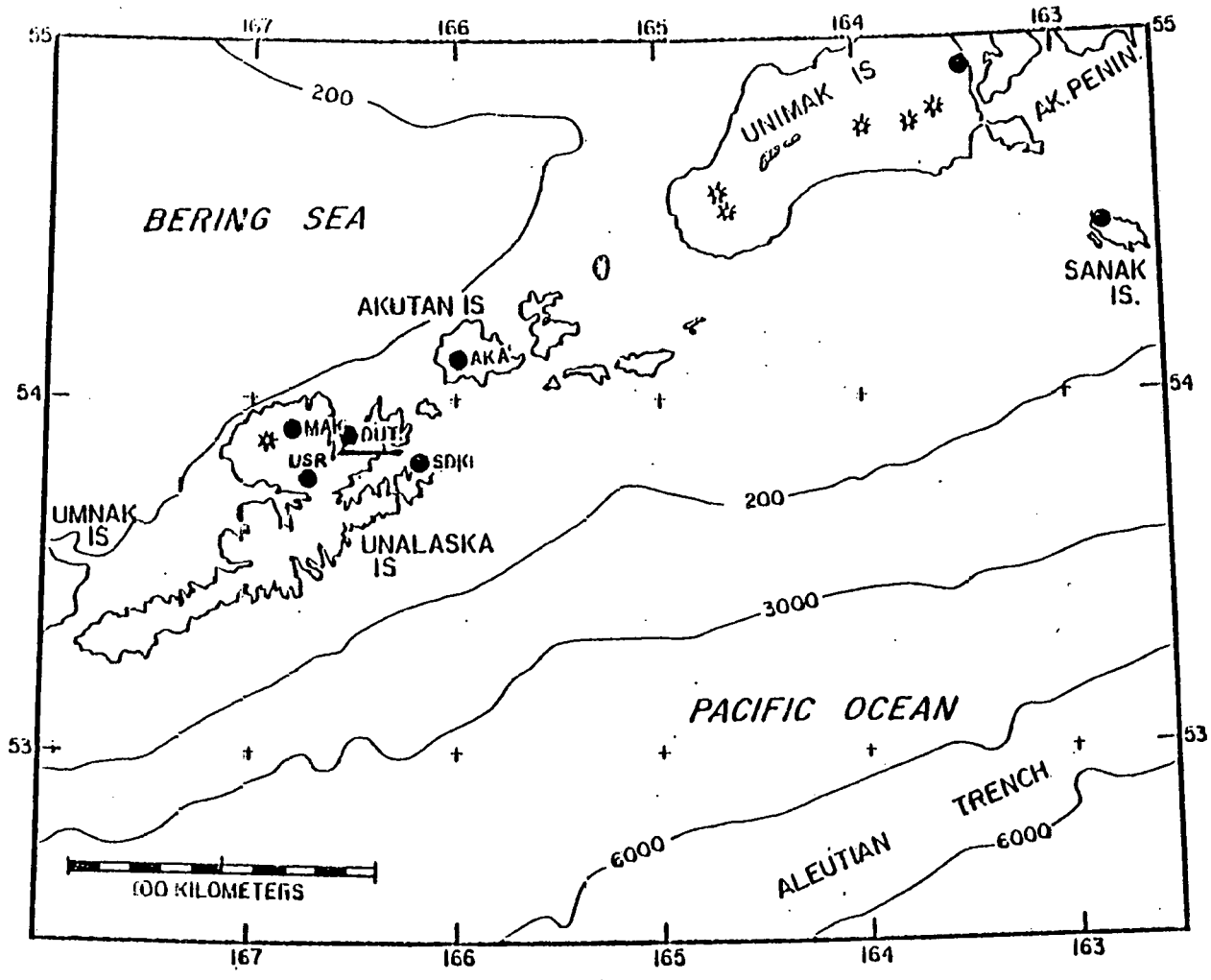

Figure 21. Unalaska Network. Remote stations (MAK, SDK, AKA, and USR) are shown by a filled cirdle, stations planned but not installed (TGD and WDL) due to weather and mechanical problems are shown by the circles enclosing a dot. The two filled circles in the upper right corner are the stations False Pass (FPS) and Sanak Island (SNK) of the Shumagin Network. The recording center for the Unalaska Network is in Dutch Harbor (DUT) shown by a filled hexagon. The sensor at each of the remote stations is a single, vertical seismometer of 1 Hz natural frequency. At DUT there are three orthogonal seismometers at 1 Hz, one vertical at 15 sec and a Kinemetrics SMA-1 strong-motion accelerograph (indicated by the heavy line under the designator code DUT). In addition to the usual short-period mode, the orthogonal set is also recorded in an intermediate period mode which is designed to span the band from 20 to .25 seconds period and to be intermediate in magnification between the short period and the strong-motion systems. All of the signals (except those of the SMA-1) are event-detected and recorded on analog magnetic tape. Two helicorder records are made to continuously monitor the system. The magnetic tapes are digitized and processed at L-DGO using the USGS PDP 11/70 data analysis system.

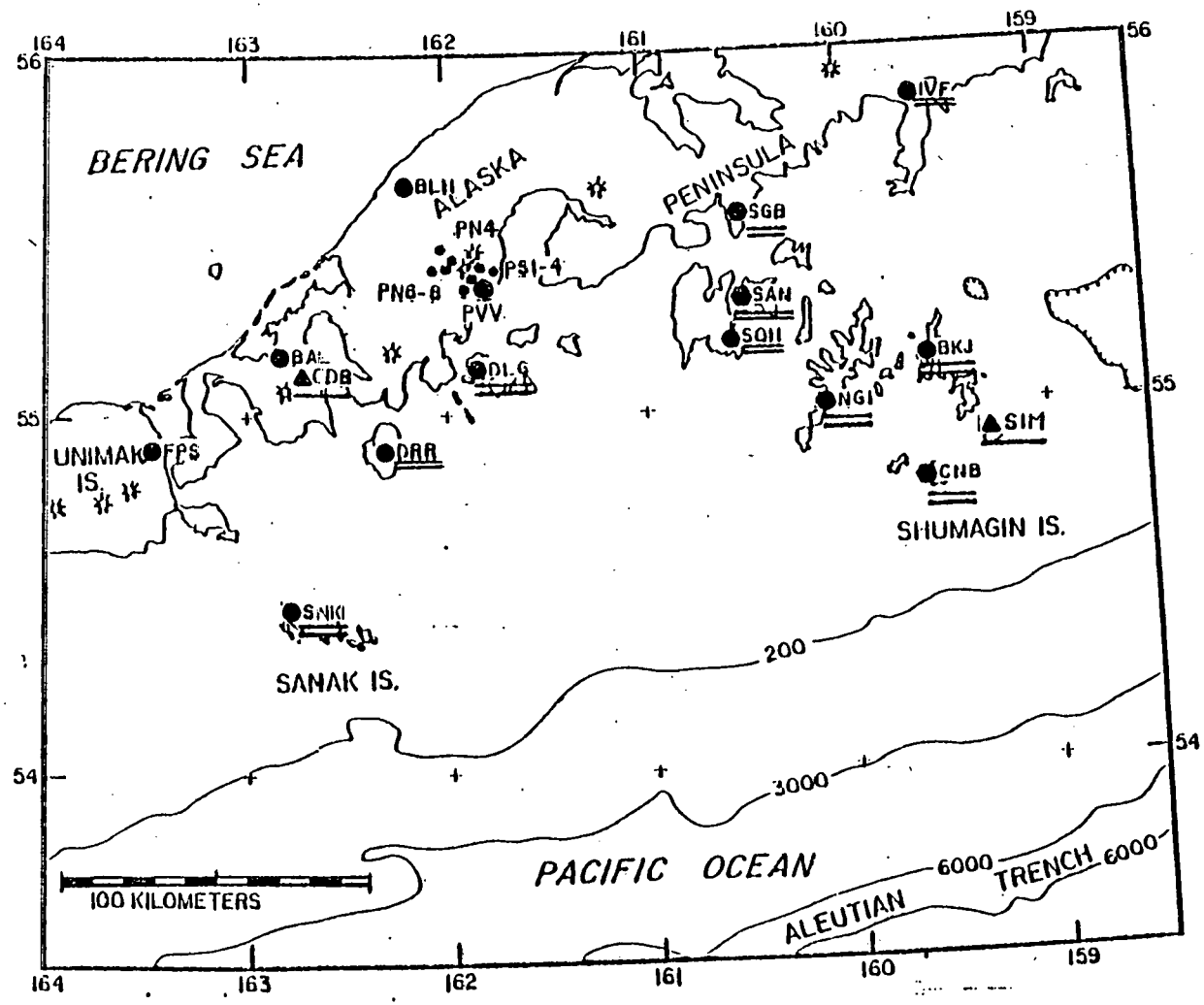

Figure 22. Shumagin Network. Remote stations with a single, vertical geophone are shown with filled circles. Stations with three orthogonal seismometers (CNB, SGB, and SAN) are shown with a filled hexagon. Network stations with SMA-1 strong-motion accelerographs are indicated by the heavy line under the designator code. Those with double underlining transmit an SMA trigger signal: when one of these SMA's is triggered, a tone is sent via the VHF telemetry system to a detector at SAN which turns on the tape recorder. The triangles at SIM and CDB indicate SMA-1's unrelated to any network station. The SAN station has three orthogonal long period seismographs as well as the short and intermediate period system similar to that at DUT (see caption from Figure 21). Signals at SAN are recorded on event detecting magnetic tape recorders (analog and digital) and 8 Helicorders; records from these devices are processed at L-DGO.

6. REFERENCES

Davies, J., L. Sykes, L. House, and K. Jacob, 1981. Shumagin seismic gap, Alaska Peninsula: History of great earthquakes, tectonic setting, and evidence for high seismic potential, J. Geophys. Res., 86(B5), 3821-3856.

Engdahl, E.R., and C.H. Scholz, 1977. A double Benioff zone beneath the central Aleutians: An unbending of the lithosphere, Geophys. Res. Lett., 4, 473-476.

Fujita, K., and H. Kanamori, 1981. Double seismic zones and stresses of intermediate depth earthquakes, Geophys. J. R. astr. Soc., 66, 131-156.

Hamaguchi, H., K. Goto, and Z. Suzuki, 1981. Double-planed structure of intermediate-depth seismic zone and thermal stress in the descending slab (abstract), IASPEI 21st Assembly, July 21-30, 1981, Dept. Geophys., University of Western Ontario, London, Ontario, Canada.

Hasegawa, A., N. Umino, and A. Takagi, 1978. Double-planed structure of the deep seismic zone in the northeastern Japan arc, Tectonophysics, 47, 43-58.

Hasegawa, A., N. Umino, A. Takagi, and Z. Suzuki, 1979. Double-planed deep seismic zone and anomalous structure in the upper mantle beneath northeastern Honshu (Japan), Tectonophysics, 57, 1-6.

House, L., and K.H. Jacob, 1982. Earthquakes, subduction, and plate deformation: Detailed seismologic observations in the Eastern Aleutian Arc, in preparation.

House, L., L.R. Sykes, J.N. Davies, and K.H. Jacob, 1981. Identification of a possible seismic gap near Unalaska Island, Eastern Aleutians, Alaska, in Earthquake Prediction, An International Review, Maurice Ewing Series 4, edited by D.W. Simpson and P.G. Richards, 81-92, AGU, Washington, D.C.

Isacks, B.L., and M. Barazangi, 1977. Geometry of Benioff zones: Lateral segmentation and downwards bending of the subducting lithosphere, in Island Arcs, Deep Sea Trenches and Back-Arc Basins, Maurice Ewing Series 1, edited by M. Talwani and W.C. Pitman III, 99-114, AGU, Washington, D.C.

Jacob, K.H., and O.J. Pérez, 1982. Seismic stress and strain from subduction beneath Alaska, in preparation.

Klein, F.W., 1978. Hypocenter location program HYPOINVERSE, part 1: Users guide to versions 1, 2, 3, and 4; part 2: Source listings and notes, U.S. Geol. Surv. Open-File Report 78-694, 114p.

Kubotera, A., 1974. Volcanic tremors at Aso Volcano, in Physical Volcanology, Developments in Solid Earth Geophysics, 6, edited by Civetta et al., Elsevier, Amsterdam.

Lahr, J.C., 1980. HYPOELLIPSE/MULTICS: A computer program for determining local earthquake hypocentral parameters, magnitude, and first motion pattern, U.S. Geol. Surv. Open-File Report 80-59, 61p.

McCann, W.R., O.J. Pérez, and L.R. Sykes, 1980. Yakataga seismic gap, southern Alaska: Seismic history and earthquake potential, Science, 207, 1309-1314.

McCollon, R.L., and R.L. Crosson, 1975. An array study of upper mantle velocity in Washington State, Bull. Seismol. Soc. Amer., 65, 467-482.

Minster, J.B., and T.H. Jordan, 1978. Present-day plate motions, J. Geophys. Res., 83, 5331-5354.

Nicholson, C., and D.W. Simpson, 1981. Routine processing of shallow earthquake locations and velocity models, EOS, Trans. AGU, 62, no. 17, p.336.

Pérez, O.J., and K.H. Jacob, 1980. Tectonic model and seismic potential of the eastern Gulf of Alaska and Yakataga seismic gap, J. Geophys. Res., 85, 7132-7150.

Reyners, M., and K. Coles, 1981. Fine structure of the dipping seismic zone and subduction mechanics in the Shumagin Islands, Alaska, submitted to J. Geophys. Res..

Samowitz, I.R., and D.W. Forsyth, 1981. Double seismic zone beneath the Mariana island arc, J. Geophys. Res., 86, 7013-7121.

Sleep, N.H., 1979. The double seismic zone in downgoing slabs and the viscosity of the mesospohere, J. Geophys. Res., 84, 4565-4571.

Sykes, L.R., 1966. The seismicity and deep structure of island arcs, J. Geophys. Res., 71, 2981-3006.

Sykes, L.R., J.B. Kisslinger, L. House, J. Davies, and K.H. Jacob, 1980. Rupture zones of great earthquakes, Alaska-Aleutian arc, 1784-1980, Science, 210, 1343-1345.

Sykes, L.R., J.B. Kisslinger, L. House, J. Davies, and K.H. Jacob, 1981. Rupture zones and repeat times of great earthquakes along the Alaska-Aleutian arc, 1784-1980, in Earthquake Prediction, An International Review, Maurice Ewing Series 4, edited by D.W. Simpson and P.G. Richards, 73-80, AGU, Washington, D.C.

Timoshenko, S.P., and J.N. Goodier, 1970. Theory of Elasticity, (3rd edition), McGraw-Hill, New York, 567p.

Toksoz, M.N., J.W. Minear, and B.R. Julian, 1971. Temperature of field and geophysical effects of a downgoing slab, J. Geophys. Res., 76, 1113-1138.

Veith, K.F., 1974. The relationship of island arc seismicity to plate tectonics, Ph.D. thesis, Southern Methodist University, 162p.

Veith, K.F., 1977. The nature of the dual zone of seismicity in the Kuriles arc, Trans. Amer. Geophys. Union, 58, 1232.

Vetter, U., and J. Minster, 1981. Pn velocity anisotropy in southern California, Bull. Seismol. Soc. Amer., 71, no. 5, 1511-1530.

Wyss, M., and J. Brune, 1967. The Alaska earthquake of 28 March 1964: A complex multiple rupture, Bull. Seismol. Soc. Amer., 57, no.5, 1017-1023.

Yang, M., M.N. Toksoz, and A.T. Smith, 1977. Thermoelastic analysis of the stresses in a subduction region (abstract), EOS, Trans. AGU, 58, 1233-1234.

7. APPENDICES

7.1 Volcano Reports from the Smithsonian Institute Prepared With Assistance of Lamont-Doherty Personnel for Eruptions of Pavlof and Shishaldin Volcanoes, Eastern Aleutian Arc

(a) For September 1980 Sequences

(b) For September 1981 Sequences

7.1.a

Pavlof Volcano, Alaska Peninsula, Alaska, U.S.A. (55.42°N, 161.90°W). All times are local (GMT – 10 h). An eruption from Pavlof November 11-12 ejected large lava fountains and ash clouds that reached 11 km altitude and may have produced lava flows.

A seismic station 10 km southwest of Pavlof registered a 2½ min burst of low-amplitude harmonic tremor beginning on November 5 at 1351. Emission of steam, ash, and some blocks from a vent high on the northeast flank started November 8 at 1047 and lasted about 5 min, without accompanying seismicity. A second burst of low-amplitude tremor occurred between 0536 and 0541 on November 9.

In contrast to the pattern observed before eruptions in 1973, 1974, 1975, and 1976, virtually no additional seismic activity was recorded until a group of seven low-frequency volcanic earthquakes occurred at about 2300 on November 10. After an explosion event appeared on seismic records at 0243 on November 11, 10 more low-frequency volcanic earthquakes were recorded between 0300 and 0400. Continuous harmonic tremor, of fairly low amplitude, began at 0608, but amplitude intensified around 0900.

Reeve Aleutian Airways pilot Everett Skinner saw rocks up to 1 m in diameter rising 10 to 30 m at 1315 on November 11. An observer in Cold Bay, 60 km to the West, noted an increase in activity about 1600. Skinner returned to the vicinity of Pavlof between 1630 and 1700, reporting lava fountaining from the summit, a black cloud hugging the volcano's upper north flank, and an eruption column reaching an estimated 6 km altitude. Between 1800 and 2000, various witnesses reported lava fountaining to a maximum height of 300 m and incandescent material moving down the north flank. A satellite image returned at 1958 shows a nearly circular plume, 15 km in diameter, north of the volcano. Activity was visible through the night from Cold Bay (see above) and the Sand Point area (50-65 km to the east northeast).

The next morning, at 0946, a satellite image revealed a plume 160 km long and almost as wide spreading north of Pavlof. Spectral analysis and weather balloon data indicate that the plume reached 8-9 km above sea level. Pilot reports on November 12 placed the top of the eruption cloud at 9 km at 1000, 6 km at 1100, and 11 km at 1400. The eruption clouds were described as varying from ash-rich to ash-poor. A helicopter crew from KENI television, Anchorage, videotaped pulses and bursts of lava fountaining, rising 150-300 m between 1600 and 1700. The fountains emerged from a preexisting vent high on the northeast flank, the only vent confirmed active during the eruption.

Very high amplitude harmonic tremor accompanied the eruption, reaching its strongest levels between 2000 on November 11 and 0700 on November 12. Tremor ceased at 1835 on November 12, at which time many B-type earthquakes began to be recorded.

By the morning of November 13, the eruption had ended. Several hundred B-type events per day were recorded November 14-15. Renewed high-amplitude tremor began November 15 at 1306, lasting until 1711. B-type earthquakes continued November 16-19, but fewer than 100/day were recorded.

Information contacts: S. McNutt and J. Davies, Lamont-Doherty Geological Observatory, Palisades, NY 10964.

Alison Till, U.S. Geological Survey, 1209 Orca St., Anchorage, AK 99501.

Jürgen Kienle, Geophysical Institute, University of Alaska, Fairbanks, AK 99701.

G. Roberts, Cold Bay Weather Station, Cold Bay, AK 99571.

Commander John Hair, Chief, Marine Environmental Branch, P O Box 3-5000 (MEP), Juneau, AK 99802.

Pavlof Volcano, Alaska Peninsula, Alaska, USA (55.42°N, 161.90°W); Shishaldin Volcano, Unimak Island, Aleutian Islands, Alaska, USA (54.75°N, 163.97°W). All times are local (GMT − 9 h). NOAA weather satellite images revealed an eruption plume emerging from Pavlof at 1030 on September 25. On the image returned at 1415, when weather clouds next permitted a clear view of the area, both Pavlof and Shishaldin (about 150 km to the southwest) were emitting plumes. At 1545, data from infrared imagery indicated that the temperature at the top of Pavlof's cloud was −55°C, corresponding to an altitude of about 9 km, and Shishaldin's cloud had reached 6–7.5-km altitude. The clouds drifted nearly due east and were still visible at 1945 when imagery showed a new plume originating from Pavlof (but not from Shishaldin). By 2215 the new plume had reached 9–10.5-km altitude and feeding from Pavlof appeared to be continuing. By 0415 the next morning the bulk of this plume had drifted to the southeast and appeared to be largely disconnected from its source, although faint traces of plume may have extended back to Pavlof. Fishermen in Pavlof Bay reported that activity continued through the night, dropping nearly 4 cm of ash on one boat. An ash sample from one of the boats was sent to the U.S. Geological Survey (USGS) in Anchorage. No certain activity could be distinguished on the satellite image returned at 0615, but there were unconfirmed reports of a renewed eruption at Pavlof by about 0700, and by 0930 the imagery again showed plumes from both Pavlof and Shishaldin. From infrared imagery, a temperature of −28°C was determined for the top of Pavlof's plume, indicating that its altitude was approximately 7.5 km. A Reeve Aleutian Airways pilot flying near Pavlof at 1000 observed a black eruption column and estimated the altitude of its top at roughly 6–7 km. He also reported incandescent material on the west flank. On the next satellite image with clear visibility, returned at 1415, a faint plume that extended to the east southeast was still connected to Pavlof, but no activity could be seen at Shishaldin. No eruption clouds have been observed on the imagery since then, and there have been no reports from pilots of renewed activity.

A visit to the Pavlof October 2–3 by Egill Hauksson and Lazlo Skinta revealed that lava had been extruded from a vent about 100 m below the summit (elevation 2518 m) and had flowed down the north northwest flank to about the 600-m level. The lava covered an area of roughly 3 km² and was 6–7 m thick at the thickest portion of the flow front, which was not advancing. A sample of the lava was sent to the Lamont-Doherty Geological Observatory. No ashfall thicknesses could be determined because of redistribution by very strong winds.

A Lamont-Doherty seismic monitoring station 7.5 km SE of Pavlof's summit recorded occasional periods of harmonic tremor and an increase in the size of B-type events beginning about 2 weeks before the eruption. However, a few days before the eruption began, both the number and size of events decreased; only five discrete shocks were recorded between 1500 on September 22 and 1500 on the 23rd, and only two during the next 24 hours, as compared to an average background level of 15–25 per day. On September 25, the day Pavlof's eruption was first observed on satellite imagery, the seismographs recorded a few more discrete events and intermittent, very low amplitude harmonic tremor. Between 2000 on September 25 and 0300 on September 26, tremor amplitude increased gradually, and by about 0330, tremor was saturating the instruments. The strongest tremor was recorded between 0500 and 0900, then amplitudes began to decrease. However, tremor remained strong and continuous until 1220 on September 27, when it declined to several-minute bursts, between which discrete events could be observed. About 100 discrete events and lower-amplitude bursts of tremor were recorded during the 24-hour period ending at 1500 on September 28. As of October 5, B-type events and bursts of harmonic tremor were continuing.

Pavlof last erupted in November 1980, ejecting ash clouds that reached 11-km altitude, large lava fountains, and a long narrow lava flow that moved down the north flank (see *SEAN Bulletin, 5,* 11). Both the 1980 and 1981 eruptions occurred from vents high on the north flank, but it was not certain at press time whether these were the same vents. Shishaldin's last reported activity was in February 1979, when pilots saw unusually strong ash emission on the 14th, 15th, and 17th.

Information contacts: Thomas Miller and James Riehle, USGS, 1209 Orca St., Anchorage, Alaska 99501; Stephen McNutt and Egill Hauksson, Department of Geological Sciences, Columbia University and Lamont-Doherty Geological Observatory, Palisades, New York, 10964; Waldo Younker, NOAA/NESS, SFSS, Box 45, Room 518-F, 701 C St., Anchorage, Alaska 99513.

7.2 Papers Published Since Last Annual Progress Report (October 1980)

(1) Nakamura, K., G. Plafker, Jacob, K.H., and J.N. Davies, 1980. A tectonic stress trajectory map of Alaska using information from volcanoes and faults, Bull. Earthquake Res. Inst., 55, Part 1, 89-100, Univ. of Tokyo.

(2) McCann, W.R., S.P. Nishenko, L.R. Sykes, and J. Krause, 1980. Seismic gaps and plate tectonics: Seismic potential for major plate boundaries, Pure Appl. Geophys., 117, 1082-1147.

(3) Perez, O.J., and K.H. Jacob, 1980. St. Elias, Alaska, earthquake of February 28, 1979: Tectonic setting, and precursory seismic pattern, Bull. Seismol. Soc. Amer., 70, 1595-1606.

(4) Sykes, L.R., J.B. Kisslinger, L. House, J. Davies, and K.H. Jacob, 1980. Rupture zones of great earthquakes, Alaska-Aleutian arc, 1784-1980, Science, 210, 1343-1345.

(5) House, L., and J. Boatwright, 1980. Investigation of two high stress-drop earthquakes in the Shumagin seismic gap, Alaska, J. Geophys. Res., 85, 7151-7165.

(6) Perez, O.J., and K.H. Jacob, 1980. Tectonic model and seismic potential of the eastern Gulf of Alaska and Yakataga seismic gap, J. Geophys. Res., 85, 7132-7150.

(7) Davies, J., L. Sykes, L. House, and K. Jacob, 1981. Shumagin seismic gap, Alaska Peninsula: History of great earthquakes, tectonic setting, and evidence for high seismic potential, J. Geophys. Res., 86(B5), 3821-3856.

(8) House, L., L.R. Sykes, J.N. Davies, and K.H. Jacobv, 1981. Identification of a possible seismic gap near Unalaska Island,

Eastern Aleutians, Alaska, in Earthquake Prediction, An International Review, Maurice Ewing Series 4, edited by D.W. Simpson and P.G. Richards, 81-92, AGU, Washington, D.C.

(9) Sykes, L.R., J.B. Kisslinger, L. House, J. Davies, and K.H. Jacob, 1981. Rupture zones and repeat times of great earthquakes along the Alaska-Aleutian arc, 1784-1980, in Earthquake Prediction, An International Review, Maurice Ewing Series 4, edited by D.W. Simpson and P.G. Richards, 73-80, AGU, Washington, D.C.

(10) Sykes, L.R., and R.C. Quittmeyer 1981. Repeat times of great earthquakes along simple plate boundaries, in Earthquake Prediction, An International Review, Maurice Ewing Series 4, edited by D.W. Simpson and P.G. Richards, 217-247, AGU, Washington, D.C.

7.3 Papers Submitted for Publication or In Press

(1) McNutt, S.R., and R.J. Beavan, 1981. Volcanic earthquakes at Pavlof Volcano, Alaska, correlated with the solid earth tides, Nature, in press.

(2) Reyners, M., and K. Coles, 1981. Fine structure of the dipping seismic zone and subduction mechanics in the Shumagin Islands, Alaska, J. Geophys. Res., in pres.

(3) McNutt, S.R., and R.J. Beavan, 1981. Correlation of the solid earth tide with volcanic earthquakes at Pavlof Volcano, Alaska, Proceedings of the 9th International Symposium on Earth Tides, New York, in press.